We are IntechOpen, the world's leading publisher of Open Access books Built by scientists, for scientists

4,800
Open access books available

122,000
International authors and editors

135M
Downloads

Our authors are among the

154
Countries delivered to

TOP 1%
most cited scientists

12.2%
Contributors from top 500 universities

CLARIVATE ANALYTICS BOOK CITATION INDEX INDEXED

WEB OF SCIENCE™

Selection of our books indexed in the Book Citation Index in Web of Science™ Core Collection (BKCI)

Interested in publishing with us?
Contact book.department@intechopen.com

Numbers displayed above are based on latest data collected.
For more information visit www.intechopen.com

1

Introduction to the Physics of Free Electron Laser and Comparison with Conventional Laser Sources

G. Dattoli[1], M. Del Franco[1], M. Labat[1], P. L. Ottaviani[2] and S. Pagnutti[3]
[1]*ENEA, Sezione FISMAT, Centro Ricerche Frascati, Rome*
[2]*INFN Sezione di Bologna*
[3]*ENEA, Sezione FISMET, Centro Ricerche Bologna*
Italy

1. Introduction

The Free Electron Laser (FEL) can be considered a laser, even though the underlying emission process does not occur in an atomic or a molecular system, with population inversion, but in a relativistic electron beam, passing through the magnetic field of an undulator. Several parameters (such as gain, saturation intensity, etc.) are common to both devices and this allows a unified description. The origin of Laser traces back to the beginning of the last century, when Planck derived the spectral distribution of the radiation from a "blackbody" source, a device absorbing all the incident radiation and emitting with a spectrum which only depends on its temperature. A perfectly reflective cavity, with a little hole, can be considered a blackbody source; the radiated energy results from the standing wave or resonant modes of this cavity. The Planck distribution law, yielding the equilibrium between a radiation at a given frequency ω and matter at a given temperature *T*, is the following:

$$I(\omega)d\omega = \frac{\hbar\omega^3}{\pi^2c^2\left[\exp\left(\frac{\hbar\omega}{kT}\right)-1\right]}d\omega \tag{1}$$

$$\hbar = \frac{\mathrm{h}}{2\pi},\ \omega = 2\pi\nu,\ \nu = \textit{frequency}\ .$$

$I(\omega)d\omega$ is the energy per unit surface, per unit time, emitted in the frequency interval $\omega, \omega + d\omega$. Its fundamental nature can be stressed by noting that it crucially depends on three constants *h, k and c* the Planck, the Boltzmann constants and the light velocity, respectively. Its derivation required the assumption that the changes in energy are not continuous, but discrete. The Plank theory prompted Bohr to make a further use of the discretization (or better quantization) concept to explain the atom stability. He assumed that the electrons, in an atomic system, are constrained on a stationary orbit, whose energetic

level is fixed and can only exchange quanta of radiation with the external environment. This point of view allowed Einstein to formulate the theory of spontaneous and stimulated emission, which paved the way to the laser concept. An atomic system with two states of energy E_1 and E_2 is shown in Fig. 1, 1 being the lower energy state.

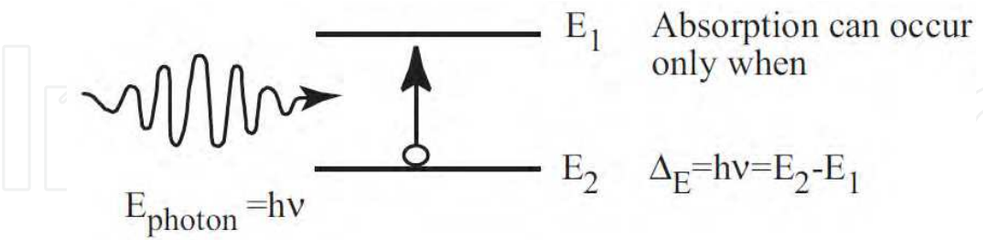

Fig. 1. Absorption process of a photon and consequent state excitation

The excitation of the system to the higher state (see Fig. 1) can result, with a probability $B_{1,2}$, from the absorption of a photon with an energy of:

$$\varepsilon = \hbar\omega,\ \omega = \frac{E_2 - E_1}{\hbar} \tag{2}$$

The principle of minimum energy requires that the system, in the excited state, decays to the lower state spontaneously, by emitting a photon of the same energy (see Fig. 2). The crucial step, made by Einstein, was the assumption that there is another process of decay, referred as stimulated, for which the transition to the lower state (see Fig. 3) occurs, with probability $B_{2,1}$, in the presence of a photon of energy equal to the energy difference between the two states as defined in Eq. (2).

We consider now a system of N atoms, among which N_1 are in the lower state and N_2 in the higher state ($N_1 + N_2 = N$), in interaction with an electromagnetic field of intensity $I(\omega)$.

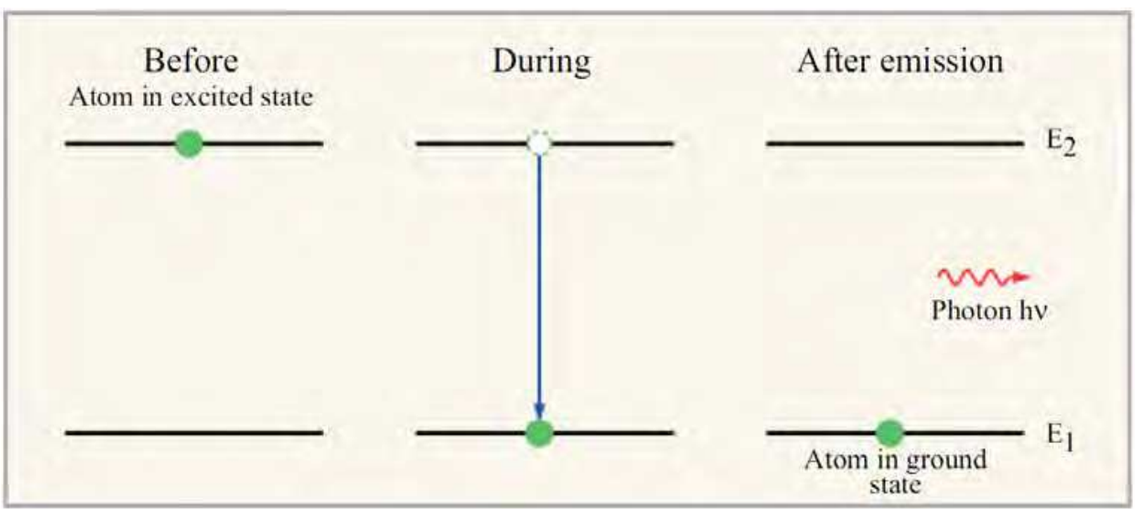

Fig. 2. Spontaneous emission process

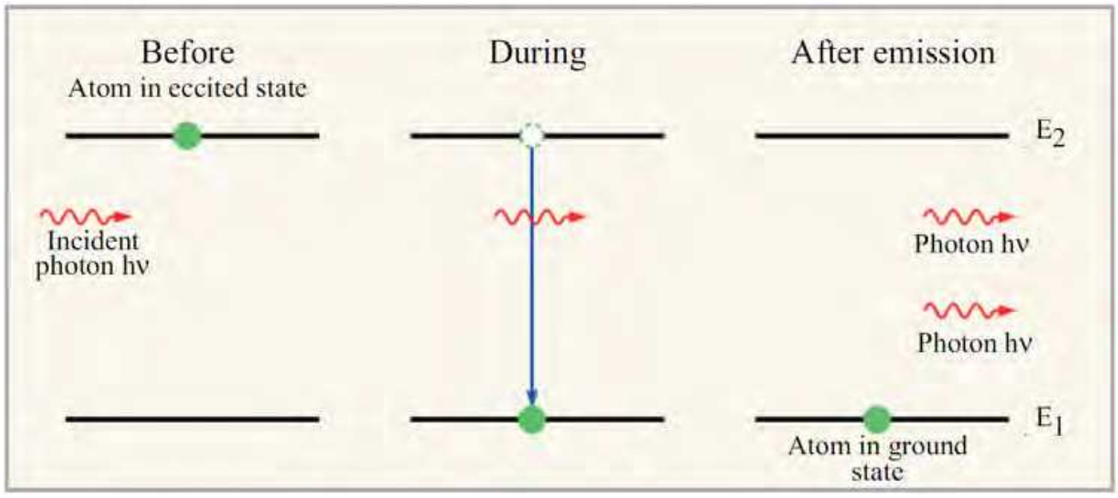

Fig. 3. Stimulated emission process

The equilibrium condition of the atomic system with the radiation is therefore given by:

$$N_1 B_{1,2} I(\omega) = N_2 B_{2,1} I(\omega) + N_2 A_{2,1} \tag{3}$$

where $A_{2,1}$ represents the spontaneous emission contribution, independent of $I(\omega)$. In the conditions of thermodynamic equilibrium at temperature T, the number of atoms per unit volume in a given state of energy E_i is described by the Boltzmann distribution law: $N_i \propto e^{-iE_i/KT}$. From this relation, one can derive the ratio $\frac{N_1}{N_2}$ in terms of energy difference and absolute temperature, namely $\frac{N_1}{N_2} = \exp\left(\frac{\hbar\omega}{kT}\right)$, which combining with Eq. (3), yields:

$$I(\omega) = \frac{A_{2,1}}{B_{1,2} exp(\frac{\hbar\omega}{kT}) - B_{2,1}} \tag{4}$$

Assuming that the absorption and stimulated emission processes are perfectly symmetric, i.e. that $B_{m,n} = B_{n,m}$, and using the Wien law, the spontaneous emission can be written as:

$$A_{n,m} = \frac{\hbar\omega^3}{\pi^2 c^2} B_{m,n} \tag{5}$$

Eq. (4) provides therefore the Planck distribution law. The importance of this result stems from the fact the Planck distribution has been derived on the basis of an equilibrium condition and on the new concepts of spontaneous and stimulated emission. The main difference between the two processes is that, in the case of the spontaneous emission, the atoms decay randomly in time and space, generating photons uncorrelated in phase and direction; in the other, the atoms decay at the same time, generating "coherent" photons, with phases and directions corresponding to those of the incident photon. Given a certain number of atoms, all (or most of them) in the higher level, one can get a substantive amplification process from one single photon (see Fig. 4).

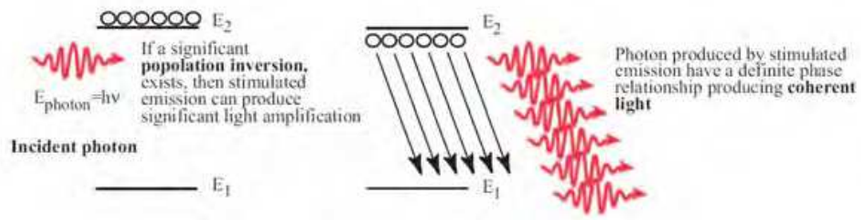

Fig. 4. Stimulated emission

We consider a medium of $N_1 + N_2 = N$ systems of two states, in interaction with an electromagnetic field with the energy of a single photon $\hbar\omega = E_2 - E_1$. During the propagation in the z direction (see Fig. 5), the variation of the number of photons n of the field is driven by a differential equation deriving from Eq. (3):

$$\frac{dn}{dz} = (N_2 - N_1)b_{1,2}n + a_{2,1}N_2 \tag{6}$$

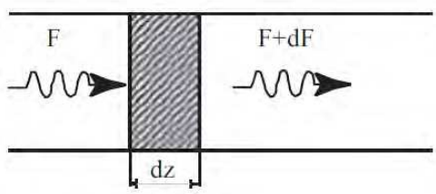

Fig. 5. Increment of the radiation

The coefficients of emission and absorption have been redefined to take into account the physical dimensions. The solution of Eq. (6) is:

$$n(z) = n_0 exp(\alpha z) + \beta \frac{exp(\alpha z) - 1}{\alpha}, \alpha = (N_2 - N_1)b_{2,1}, \beta = a_{1,2}N_2 \tag{7}$$

where n_0 is the initial number of photons of the field. Eq. (7) consists of two parts, and one (the spontaneous emission term) is independent of the initial number of photons. We consider the case in which the spontaneous emission contribution can be neglected. If $N_2 < N_1$, i.e. if there are less atoms in the excited than in the ground state, then $\alpha < 0$ and Eq. (7) becomes: $n(z) = n_0 exp(-|\alpha| z)$, corresponding to the Beer-Lambert law of absorption and the coefficient α can be interpreted as a coefficient of linear absorption. When $N_2 = N_1$, the number of photons remains constant. The amplification is possible if $N_2 > N_1$, i.e. when a population inversion has occurred (namely the system has been brought to the "excited" state through some mechanism). In this case, the coefficient α is understood as the small signal gain coefficient. The amplification can be seen as a chain reaction: a photon causes the decay of the excited state, creating a "clone", and, following the same process, both lead to the "cloning" of other two photons, and so on. Adding the spontaneous emission, the chain can be started without the need of an external field.

These few introductory remarks provide the elements of the light amplification, we will see how it can be implemented to realize a laser oscillator.

2. Laser oscillator

The radiation amplification, based on the stimulated emission mechanism, requires an active medium in which population inversion occurs and an environment which can provide a feedback to maintain the system in operation as an oscillator (see Fig. 6).

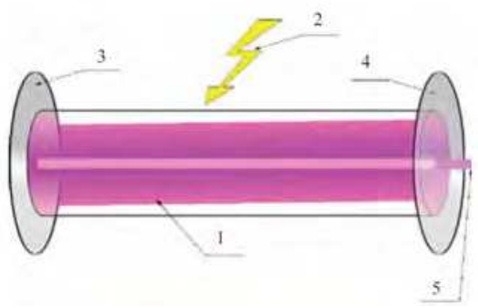

Fig. 6. Components of an oscillator laser: 1) Optical active medium, 2) Energy delivered to the optical medium, 3) Mirror, 4) Semi-reflective mirror, 5) Output laser beam

Without entering into the details of the population inversion mechanism, we can notice that it cannot be obtained simply by heating the active medium. Indeed, if we consider a two states system, the electrons obey the statistics of Fermi-Dirac and we have:

$$\frac{N_2}{N_1} = \frac{1}{\exp\left(\frac{\hbar\omega}{kT}\right)+1} \tag{8}$$

The population inversion process is not the result of a heating. At a temperature close to 0° K, the higher state is depopulated while at high temperature ($T \to +\infty$) $\frac{N_2}{N_1} = \frac{1}{2}$, i.e. the two states are equally populated. An extensively used mechanism for population inversion is the optical pumping: the active medium is slightly more complex than a two states system, which remains a convenient abstraction, but hardly actually feasible.

Since the spontaneous emission is essentially isotropic (see Fig. 7), a first direction selection can be operated by embedding the medium in an optical cavity, consisting, in its most simple configuration of two facing mirrors.

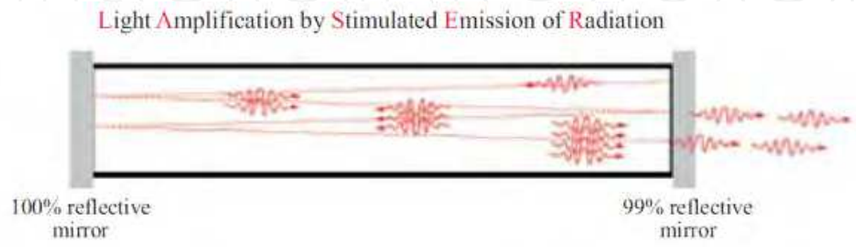

Fig. 7. Selection of the transverse mode in the optical cavity

The emitted photons result selected according to their direction, increasing the spatial coherence of the radiation at each pass in the cavity. Being assumed the existence of a gain,

one expects the radiation intensity to increase and that, at each reflection on the semi-reflective mirror, a fraction of this radiation is extracted off the cavity. Since only a part of the radiation is reflected, the evolution of the system will strongly depend on the losses of the cavity and we can expect a saturation mechanism that will drive the system to an equilibrium state. As for other physical systems, the saturation mechanism is nonlinear and controlled by the radiation intensity itself. We can now write the rate equations, i.e. the evolution equations of the laser intensity inside the cavity:

$$I_{n+1} - I_n = [(1-\eta)G(I_n) - 1]I_n \tag{9}$$

n represents the number of round trips inside the optical cavity and η the cavity losses (we do not yet distinguish the active and the passive [1] losses, so that η are the total losses). In order to take into account the effects of saturation, we assume that the gain $G(I)$ is a decreasing function of the intensity, namely

$$G(I) = \frac{g}{1 + \frac{I}{I_s}} \tag{10}$$

I_s, introduced in a phenomenological way, is a quantity of paramount importance representing the saturation intensity. For $I = I_s$, the gain corresponds to one half of the small signal gain g, which we no longer refer to as α to take into account the fact that the active medium is not a simple two sates system. Using the following approximation

$$I_{n+1} - I_n \cong T_R \frac{dI}{d\tau} \tag{11}$$

Equation (11) can be rewritten in terms of a differential equation:

$$\frac{dI}{d\tau} = [(1-\eta)G(I) - \eta]I. \tag{12}$$

τ is a dimensionless time related to the actual time t and to the length of the optical cavity L_c according to: $\tau = \frac{t}{T_R}$, $T_R = \frac{2L_c}{c}$, with T_R the duration of a round trip in the cavity. Transforming Eq. (12) into:

$$\frac{dX}{g[(1-\eta)\frac{1}{1+X} - r]X} = d\tau \tag{13}$$

$$X = \frac{I}{I_s}, r = \frac{\eta}{g}$$

it becomes obvious that for $X << 1$, i.e. far from saturation, the intensity evolves exponentially:

[1]The active losses correspond to the transmission of the radiation to the external environment, while the passive losses correspond to the absorption of the radiation by the medium and the cavity mirrors.

$$X = X_0 exp([(1-\eta)g - \eta]\tau) \tag{14}$$

It is also obvious that the equilibrium ($\frac{dX}{d\tau}$ = 0) is reached when the intensity in the cavity is such that $G(I) = \frac{\eta}{1-\eta}$ and therefore

$$I_E = [\frac{1-\eta}{\eta} g - 1] I_s \tag{15}$$

Since in most cases $\eta << 1$, the extracted power at equilibrium (assuming that the losses are only active losses) is given by:

$$I_{out} = \eta I_E \cong g I_s \tag{16}$$

This relation is an additional evidence of the importance of the saturation intensity, which along with the gain defines the power which can be extracted from the cavity. The evolution of the laser power inside the cavity as a function of the number of round trips is reported in Fig. 8.

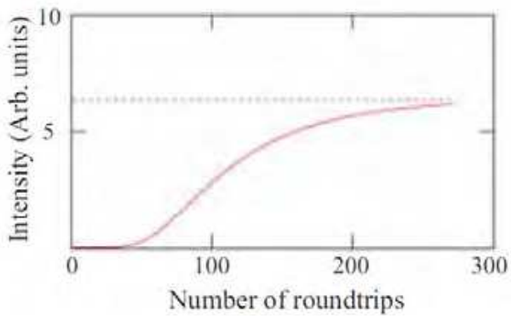

Fig. 8. Laser intensity (arb. unit) vs round trip number for *g*=15% and *h*=2%

The intensity first increases exponentially and then slows because of the saturation mechanism. When the gain equals the losses, the system reaches a stationary state and the power can be extracted off the cavity.

Despite not mentioning it before, the population inversion requires a sufficient level of power, which we refer to as pump, that will be further partially transformed into laser power. The ratio between the extracted laser power and the pump power represents the efficiency of the system.

We have seen that the optical cavity is an essential element of an oscillator, since it confines the electromagnetic radiation, selects the transverse and longitudinal modes, thus creating the spatial and temporal coherence of the radiation.

The radiation field inside the optical cavity, whose components have a small angle with respect to the cavity axis, is successively reflected by the mirrors. This enables to select the components travelling in a direction parallel to the cavity axis. The interfering of the waves in the cavity leads to the formation of stationary waves at given frequencies, depending on the distance between the mirrors. In the case of planar and parallel mirrors, separated by a

distance L, the stationary condition for the wave frequencies is: $\nu_n = n\frac{c}{2L}$, n being integer. The various frequencies obtained, varying n, are referred as longitudinal modes of the cavity. For each longitudinal mode, various transverse sections are possible, which modify the transverse intensity distribution in the plans perpendicular to the optical axis. Those are referred as transverse modes. From a conceptual point of view, an optical cavity consists of two parallel mirrors (see Fig. 9).

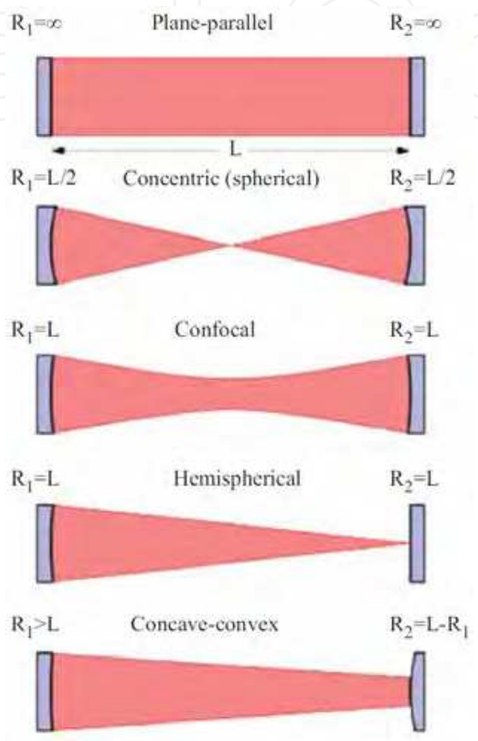

Fig. 9. Examples of optical cavities

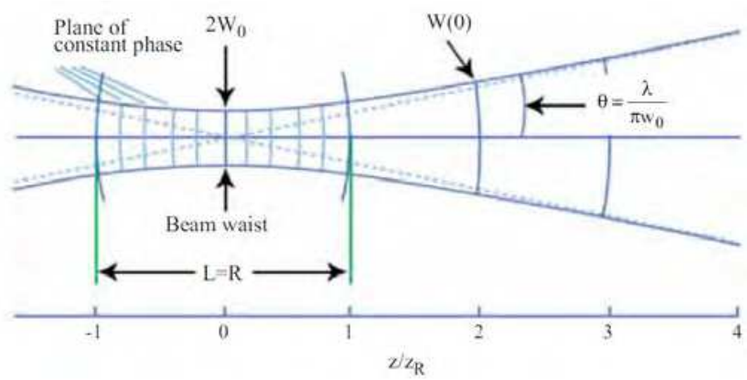

Fig. 10. Gauss-Hermite mode and main reference quantities

The mirrors configuration sets the field shape inside the cavity, as illustrated in Fig. 9. Two flat mirrors, i.e. with an infinite radius of curvature, lead to a constant transverse mode distribution. When the mirrors are confocal, the transverse mode has a parabolic

longitudinal profile, which we will discuss more in details later. Additional configurations are shown in Fig. 9. In the case of a confocal cavity, the transverse modes are the Gauss-Hermite modes and, as previously mentioned, the longitudinal profile of the mode is parabolic (see Fig. 10).

The fundamental mode corresponds to a Gaussian distribution defined as:

$$I(r,z) = I_0(\frac{w_0}{w(z)})^2 e^{-\frac{2r^2}{w(z)^2}}, \tag{17}$$

where r is the distance to the axis, w is the rms spot size of the transverse mode:

$$w(z) = w_0[1+(\frac{z}{z_R})^2] \ , \ w_0 = \sqrt{\frac{\lambda L}{2}} \ , \ z_R = \frac{\pi w_0^2}{\lambda} \tag{18}$$

w_0 is the beam waist, i.e. the minimum optical beam transverse dimension, z_R the Rayleigh length, corresponding to the distance for which $w(z) = \sqrt{2}w_0$. For the fundamental mode, $z_R = L/2$. The divergence of the mode is related to the former parameters according to:

$$\theta = \frac{\lambda}{\pi w_0^2} \tag{19}$$

θ is referred as the angle of diffraction in the far field approximation.

The longitudinal modes are equally separated in frequency by Δf, which depends on the cavity length according to:

$$\Delta f = \frac{2c}{L} \tag{20}$$

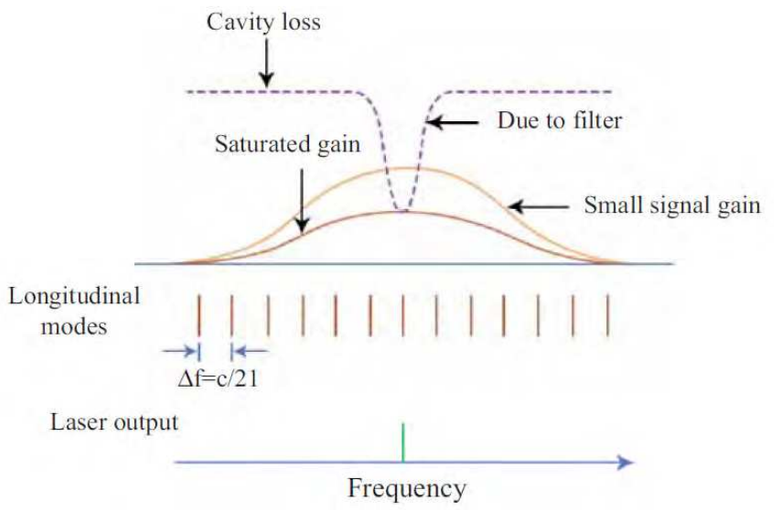

Fig. 11. Gain and loss spectra, longitudinal mode locations, and laser output for single mode laser operation

The gain bandwidth of the active medium performs the mode selection and therefore allows the amplification of the modes within this bandwidth only. Those modes oscillate independently with random phase and beating. A longitudinal mode-locking enables to fix the longitudinal modes phases so that they all oscillate with one given phase [2]. It seems obvious that, in theory, varying the losses and therefore the gain profile would allow to suppress the competition in between modes and choose for instance the one with higher gain, as illustrated in Fig. 11.

But it's also obvious that this is obtained to the detriment of the output laser power. We will now discuss alternative and less drastic methods to suppress the destructive mode competition using the previously mentioned mode-locking.

In a mode-locked laser, the output radiation does not fluctuate in a chaotic manner. It consists of a periodic train of pulses (see Fig. 12), with specific duration and temporal separation.

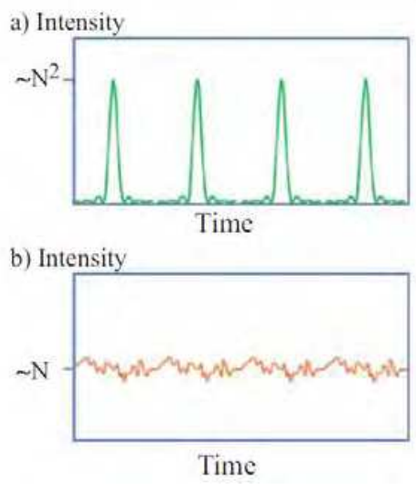

Fig. 12. Gain and loss spectra, longitudinal mode locations, and laser output for single mode laser operation(a) Mode-locked laser output with constant mode phase. (b) Laser output with randomly phased modes

We consider an electromagnetic field in an optical cavity consisting of N_m longitudinal modes locked in phase with a Δf frequency gap[2]:

$$A(z,t) = E_0 \sum_{m=-\frac{N_m-1}{2}}^{m=\frac{N_m-1}{2}} e^{2\pi i m \Delta f (t-z/c)} \tag{21}$$

For simplicity, we assumed that all the modes have the same amplitude E_0. The sum can be performed using the identity $\sum_{m=0}^{m=q-1} a^m = \frac{a^q - 1}{a-1}$, which leads to:

[2]One can notice that the frequency gap is not always the one given in Eq. (30). It can be larger if some modes are suppresses using for instance an etalon.

$$A(z,t) = E_0 \frac{sin[\pi N_m \Delta f(t - z/c)]}{sin[\pi \Delta f(t - z/c)]} \tag{22}$$

The intensity of the laser is defined as the squared moduleus of the former expression, which gives, at z =0:

$$I(t) \propto E_0^2 [\frac{sin[\pi N_m \Delta f.t]}{sin[\pi \Delta f.t]}]^2 \tag{23}$$

The result of Eq. (23) is illustrated in Fig. 12. The radiation consists of a train of peaks, separated by a distance $T = \frac{1}{\Delta f}$ with a width $\frac{1}{N_m \Delta f}$. The intensity of the peaks is proportional to the square of the number of involved modes $I_p \propto N_m^2 E_0^2$, while the average intensity is proportional to N_m, i.e. $I_M \propto N_m E_0^2$. Finally, it is important to notice that in the case of random phases, the output laser intensity corresponds to the average intensity of the mode-locked laser and that the fluctuations have a correlation time equal to the duration of one single pulse of the mode-locked laser. Since the former remarks are of notable interest for the laser applications and for further discussions, we provide with additional precisions on the radiation pulse train presented in Fig. 13.

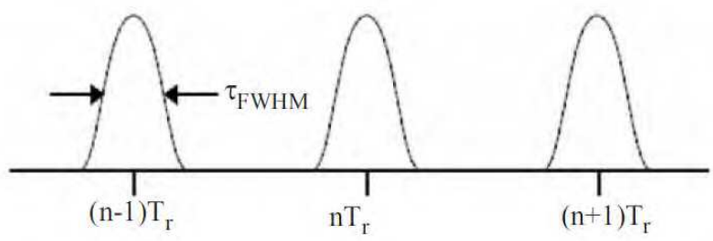

Fig. 13. Periodic pulse train

The train is characterized by an energy per pulse E_p, a delay between pulses T_p, a pulse duration δ_T (full width half maximum), an average power P_m and a peak power P_p [3]. All these quantities are linked as it follows: $P_p = \frac{E_p}{\delta_\tau}$, $P_m = P_p \frac{\delta_\tau}{T_R}$, the ratio $\frac{\delta_\tau}{T_R}$ corresponds to the duty cycle. The mode-locking techniques allow to generate ultra-short pulses.

Laser devices are usually said to provide light with temporal and spatial coherence.

The temporal coherence is a measure of the degree of mono-chromaticity of an electromagnetic wave. As a consequence, we can write:

$$\tau_c \Delta f \cong 1 \tag{24}$$

[3]We recall that the electric field is $E_p = \sqrt{2 Z_0 I_p}$, with $I_p = \frac{P_p}{A_{eff}}$ the peak intensity and A_{eff} the effective area of the optical mode, and Z_0 is the vacuum impedance.

In the case of a mode-locked laser, the coherence time is essentially given by the distance in between the radiation packets. The coherence length l_c can be calculated using Eq. (24):

$$l_c (= c\tau_c) \cong \frac{\lambda^2}{\Delta\lambda} \tag{25}$$

The spatial coherence of a wave is the measurement of the temporal auto-correlation between two different points of a same transverse plane of the wave (see Fig. 14).

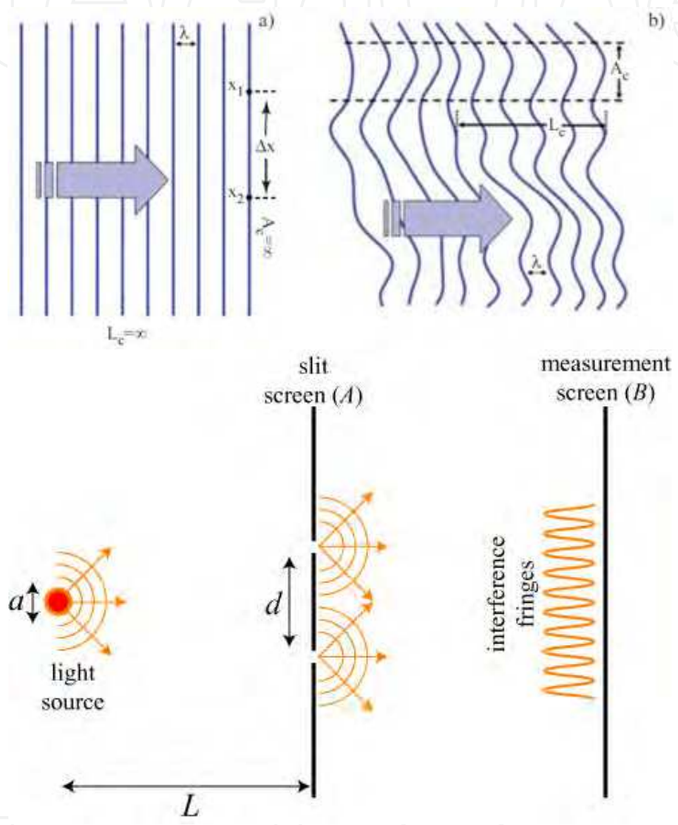

Fig. 14. Examples of wave-fronts with a) infinite and b) finite coherence length c) Coherence area

The spatially coherent part, belonging to the so called coherent area, of a wave passing through a slit produces a diffraction figure. The concept of coherence area can be quantified using the Van Cittert Zernike theorem, which states that the coherence area of a light source is given by:

$$S_c \cong \frac{L^2\lambda^2}{\pi a^2}$$

with L the distance to the source and d its diameter.

The former discussion allowed to give a general idea of the issues relative to conventional lasers. We will now discuss analogous issues relevant to FEL devices.

3. The free electron laser

In this and in the forthcoming sections we will discuss laser devices operating with an active medium, consisting of free relativistic electrons [3,5]. A few notions and a glossary of relativistic kinematics are therefore necessary. The total energy E of a particle of mass m moving with a velocity υ is given by:

$$E = m_0 \gamma c^2, \gamma = \frac{1}{\sqrt{1-\beta^2}}, \beta = \frac{v}{c}. \tag{26}$$

β is the reduced velocity and γ the relativistic factor. The total energy corresponds to the sum of the kinetic and mass energy, the mass energy being given by $m_0 c^2$. The factor γ is a measure of the particle energy, and γ-1 of the kinetic energy. In addition: $\beta = \sqrt{1-\frac{1}{\gamma^2}}$.

In the high energy case $\gamma >> 1$, the reduced velocity becomes $\beta \cong 1 - \frac{1}{2\gamma^2}$

and the particle is said "ultra-relativistic".

We now consider the main characteristics of the electrons: a charge $|e| \cong 1.6 \times 10^{-19}$ C and a mass $m_e \cong 0.51$ MeV (1 MeV=10^6 eV, 1 eV=1.6×10^{-19} J). The adjective relativistic is used when the kinetic energy of the electrons is of the order of a few MeV. Finally, a charged particle beam is associated to a power equal to the product of its energy with its current:

$$P(MW) = I(A)E(MeV). \tag{27}$$

A 20 MeV beam with a current of 2 A has a power of 40 MW. Such power is delivered to the beam by the accelerator. From now on, we will refer to LINAC accelerator, i.e. linear accelerators, where the acceleration is performed in radiofrequency cavities. The electron beam power corresponds in the case of free electron lasers, to the pump power in the case of conventional lasers.

Free electrons passing through a magnetic field produces flashes of Bremsstrahlung radiation. Synchrotron light sources rely on this process. We consider the case of a magnetic field delivered by an undulator:

$$\vec{B} = B_0 (0, sin(\frac{2\pi z}{\lambda_u}), 0) \tag{28}$$

Such field is oscillating in the vertical direction with a peak value B_0 and a periodicity λ_u. It can be obtained with two series of magnets with alternative *N-S* orientation, as illustrated in Fig. 15.

The Lorentz force, due to the undulator field, introduces a transverse component in the electron motion, initially exclusively longitudinal. The electron motion in the magnet is governed by (Gaussian units):

$$\frac{d\vec{p}}{dt} = -\frac{e}{c}\vec{v} \times \vec{B}. \tag{29}$$

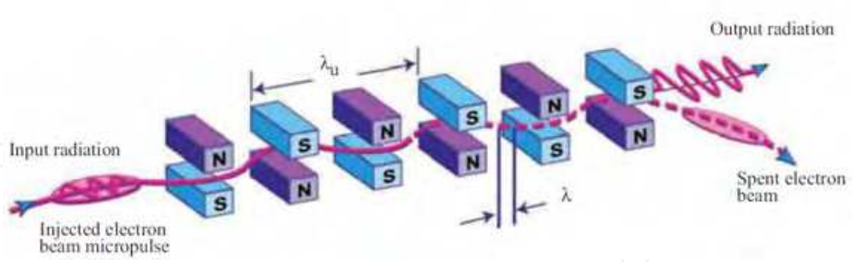

Fig. 15. Electron motion in an undulator

Averaging over one undulator period, one can derive the transverse and longitudinal velocities:

$$v_x \cong \frac{cK}{\sqrt{2}\gamma}\ ,\ v_z \cong c[1-\frac{1}{2\gamma *^2}]\ ,\ \gamma * = \frac{\gamma}{\sqrt{1+\frac{K^2}{2}}}, K = \frac{eB_0\lambda_u}{2\pi m_0 c^2}$$

The *K* parameter is introduced to take into account the effect of the transverse motion on the longitudinal velocity. The electrons moving in the undulator emits radiation and this process can be viewed as a kind of spontaneous emission, The frequency selection mechanism can be understood by referring to Fig. 16.

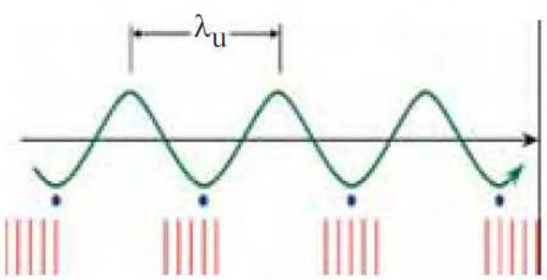

Fig. 16. Phase advance of the radiation with respect to the electrons

After one undulator period, the emitted radiation, travelling at the light velocity, has slept ahead of the electron beam by a quantity

$$\delta \sim (c - v_z)\frac{\lambda_u}{c} = \frac{\lambda_u}{2\gamma^2}\left(1 + K^2/2\right) \tag{30}$$

Since δ represents a phase advance of the electromagnetic wave, constructive interference with the radiation emitted at the next undulator period, requires the condition:

$$\delta = n\lambda, \tag{31}$$

n being an integer. From Equation (30) and Eq. (31) finally comes the definition of the undulator radiation wavelength:

$$\lambda_n = \frac{\lambda_u}{2n\gamma^2}\left(1+\frac{K^2}{2}\right) \tag{32}$$

n=1 represents the fundamental wavelength, while n>1 represent the higher harmonics. In a first step, we just consider the radiation on the fundamental and we try to characterize it, giving an evaluation of its relative bandwidth. The radiation pulse at the end of the undulator has a structure of a step function with a length $N\delta$, corresponding to a pulse duration $\Delta\tau$ of: $\Delta\tau \cong \frac{N\delta}{c}$, the corresponding spectral distribution is given by the Fourier transform of this pulse (see Fig. 17), and the spectral width $\Delta\omega$ results defined according to the Parseval relation $\Delta\tau\Delta\omega \cong \pi$.

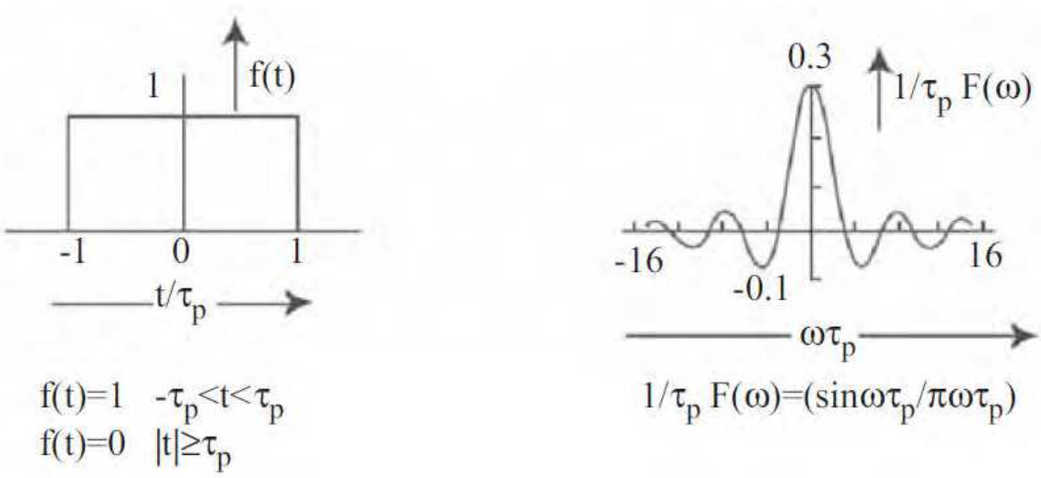

Fig. 17. Step function and corresponding Fourier transform

Thus getting for the relative bandwidth

$$\frac{\Delta\omega}{\omega} = \frac{1}{2N} \tag{33}$$

The spectral intensity profile of the radiation emitted by a single undulator is therefore just given by

$$f(\nu) \propto \left[\frac{sin(\frac{\nu}{2})}{\frac{\nu}{2}}\right]^2 \quad \nu = 2\pi N\frac{\omega-\omega_0}{\omega_0} \tag{34}$$

$f(\nu)$ is illustrated in Fig. 18 and can also be written as:

$$f(\nu) = 2Re\left[\int_0^1 (1-t)e^{-i\nu t}dt\right] \tag{35}$$

ν, the so-called detuning, is a very useful parameter, which is used to define the spectral profile with respect to the central reference wavelength. Since ν is a dimensionless parameter, the width of the profile at half of the maximum intensity is close to 2π.

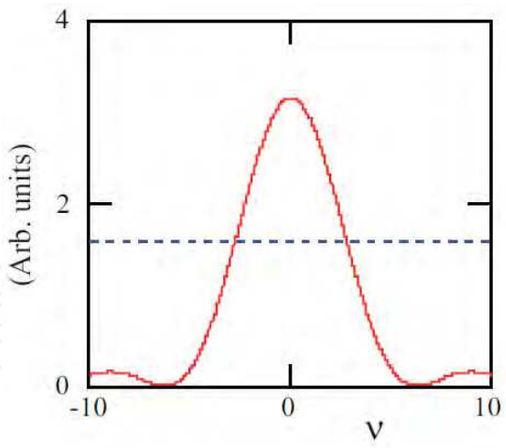

Fig. 18. Function $f(\nu)$

An oscillator FEL is similar to a conventional laser oscillator. Indeed, we find again a spontaneous emission process from a free electron beam in an optical cavity, the storing of the radiation inside the cavity, and the amplification of this radiation throughout a mechanism of stimulated emission. Fig. 19 also shows that during the interaction between the electrons and the radiation, the electron beam is being modulated in energy which results in a spatial modulation (bunching) at the radiation wavelength.

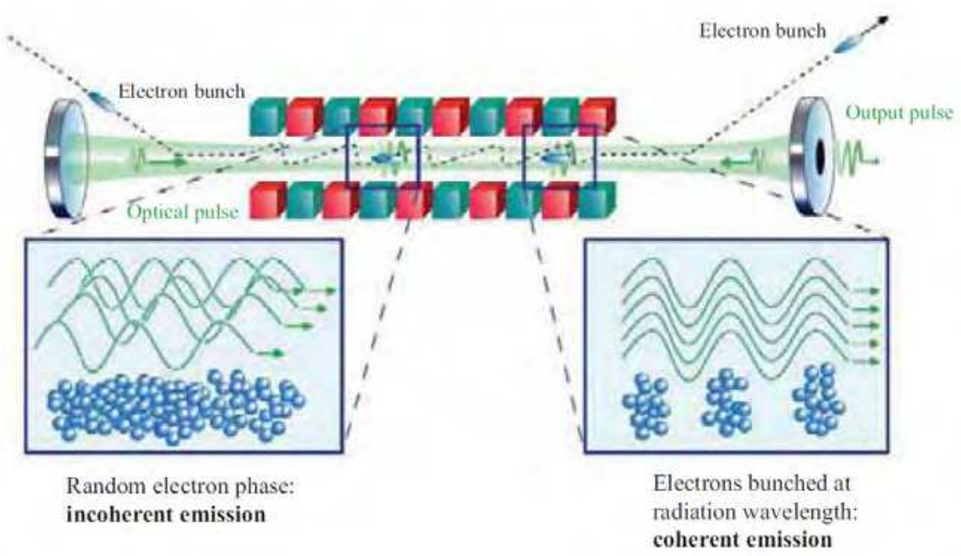

Fig. 19. Oscillator FEL

This modulation enables the production of coherent radiation. The mechanism of interaction in between the electrons and the radiation of a FEL can be considered as the combination of two competing effects:

Energy loss from the electron and then amplification of the incident photon, absorption of the stimulating photons with consequent yielding of energy to the electrons.

Such mechanism can be understood quite easily using a reference system in which the electrons are nonrelativistic. In such system, the electrons see two electromagnetic fields: the laser field travelling in the same direction, and the undulator field, which proceeds in the opposite direction ("Virtual quanta" model of Weizsacker and Williams). In Figure 20, we reported the processes of stimulated emission and absorption, similar to the processes of stimulated emission in conventional lasers.

1. the stimulated absorption can be interpreted as a backward scattering of the photons by the laser field. The electrons gain energy, which corresponds to a negative gain;
2. the stimulated emission can be interpreted as a forward scattering of the photons by the undulator field, with a frequency close to the laser frequency. The electrons loose energy, corresponding to a positive gain.

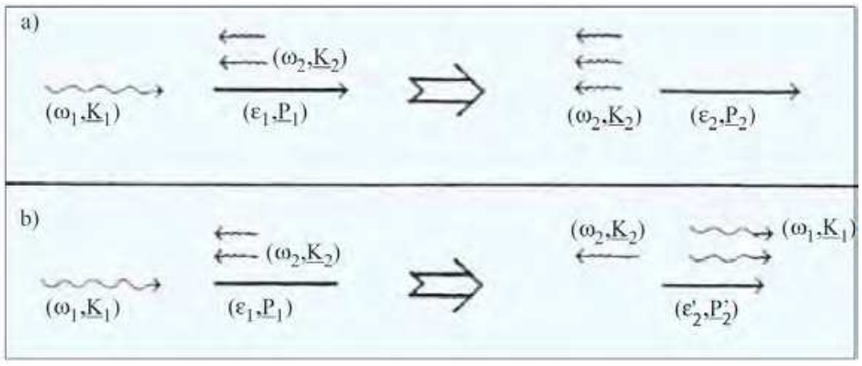

Fig. 20. Stimulated emission and absorption processes, similar to the stimulated emission process in the case of conventional lasers. $\omega_1=c/k_1$ /= laser frequency; $\omega_2=c/k_2$ /= undulator radiation frequency; ε_1,p_1= initial energy and moment of the electrons; ε_2,p_2= final energy and moment of the electrons. a) Backward stimulated scattering (negative gain). b) Forward stimulated scattering (positive gain

The spontaneous emission process is interpreted using Fig. 20 as the scattering of "undulator photons", without the presence of co-propagating electrons.

Within such a context the gain process can be viewed as the balance between stimulated absorption and emission processes, namely

$$G(\nu) \propto f(\nu_+) - f(\nu_-) \tag{36}$$

$f(\nu_{+/-})$ refers to the cases illustrated in the Figure, to emission and absorption.

Since $\nu_+ - \nu_- \propto \delta E_{rec}$, where δE_{rec} represents the energy loss of one single electron via recoiling, the expansion of Eq.(36) at the lowest order leads to (this assumption holds for low gain devices as we will discuss later):

$$G(\nu) \propto -\frac{\delta f(\nu)}{\delta \nu} \tag{37}$$

Taking into account that the radiation is emitted by an electron beam at a given current, the gain can be eventually expressed as follows

$$G(\nu) = -\pi g_0 \frac{\delta f(\nu)}{\delta \nu} = 2\pi g_0 \int_0^1 t(1-t)sin(\nu t)dt \ , \ g_0 = 4\pi \frac{|J|}{I_0}(\frac{N}{\gamma})^3(\lambda_u K^* f_b)^2$$

$$I_0 = \frac{4\pi}{Z_0 c}\frac{m_e c^3}{e} = 1.7045.10^4 A \ , \ f_b = J_0(\frac{K^{*2}}{2(1+K^{*2})}) - J_1(\frac{K^{*2}}{2(1+K^{*2})}) \quad K^* = \frac{K}{\sqrt{2}} \tag{38}$$

g_0 is the small signal gain coefficient, I_0 the Alfven current. The gain curve is reported in Fig. 21 (one can note that the maximum of the gain does not correspond to the maximum of the spontaneous emission intensity, but located at $\nu_0 \cong 2.6$). J is the current density of the electron beam and f_b the Bessel factor which takes into account the non-perfectly sinusoidal trajectory of the electrons in the linear polarized undulator.

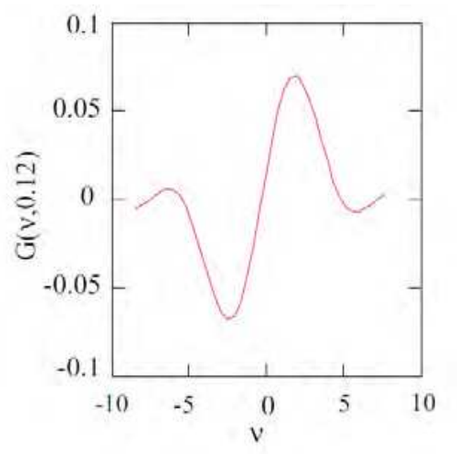

Fig. 21. FEL gain curve

It is worth mentioning that the gain curve is asymmetric. It consists of one part of positive gain and one part of absorption where the electrons, instead of giving energy to the radiation, absorb some energy from the radiation.

Now that the existence of a gain is clarified, we will determine the saturation intensity. The FEL process consists in a power transfer from the electron beam to the laser. The gain curve is asymmetric but the FEL process is maintained until the Kinematic conditions are such that a positive gain is guaranteed and that a sort of saturation is reached. The energy loss can be deduced from the width of the positive gain region, related to the detuning parameter (see Fig. 33 and Eq. (36)) by:

$$\Delta\nu \cong 4\pi N \frac{\Delta\gamma}{\gamma} \cong 2\pi \tag{39}$$

This equation yields the energy variation of the electron beam induced by the FEL interaction:

$$\frac{\Delta\gamma}{\gamma} \cong \frac{1}{2N} \tag{40}$$

We finally get the expression of the power, transferred from the radiation to the electrons (see Eq. (27)):

$$P_L \cong \frac{P_E}{2N} \tag{41}$$

According to what we discussed for conventional lasers and assuming that a similar dynamics is valid in the case of FEL, the saturation intensity can be expressed as:

$$I_S \cong \frac{I_E}{2Ng_0},\ I_E = \frac{|J|E}{e}$$

or in more practical units:

$$I_S[\frac{MW}{cm^2}] = 6.9312.10^2 \frac{1}{2}(\frac{\gamma}{N})^4(\lambda_u[cm]K^* f_b)^{-2} \tag{42}$$

In conclusion, we demonstrated that an oscillator FEL behaves like a conventional oscillator laser and therefore that most of the relevant theoretical description can be applied to the FEL.

4. FEL Oscillator model

In the former paragraph, we have shown a full parallel (in terms of gain and saturation intensity) between FEL and conventional lasers. Pursuing the analogy we can write the saturation of the FEL gain as (we impose an upper limit on the small signal gain coefficient to fix the limit of validity of this treatment)

$$\begin{aligned} &G(X) = \frac{G_M}{F(X)}, X = \frac{I}{I_s} \\ &G_M = 0.85g_0, \text{ for } g_0 \le 0.3 \end{aligned} \tag{43}$$

G_M represents the maximum gain calculated at $\nu_0 \cong 2.6$ and:

$$F(X) = 1 + \alpha X + \beta X^2, \alpha + \beta = 1, \alpha = 2(\sqrt{2} - 1), \beta = 3 - 2\sqrt{2} \tag{44}$$

One can notice that in the case of the FEL, the saturation results slightly different from the conventional laser (presence of a quadratic term), but this is just a technical detail which does not modify the physics of the process. The use of rate equations as defined in Eq .(9) enables to obtain the evolution of the laser power in the cavity as

$$I_{r+1} - I_r = [(1-\eta)G(X_r) - \eta]I_r, \tag{45}$$

As already seen, the signal increases initially in the exponential mode, then the increase slows down and finally stops (or nearly) when the gain equals the losses. The equilibrium power in the cavity is obtained from the condition $I_{r+1} = I_r$, which implies:

$$G(X_e) = \frac{\eta}{1-\eta} \tag{46}$$

Together with Eq. (43) and (44), this leads to the expression of the equilibrium intensity in the cavity:

$$I_e = (\sqrt{2}+1)(\sqrt{\frac{1-\eta}{\eta}G_M}-1)I_S \tag{47}$$

The solution of Eq. (45), (46) and (47) can be written as:

$$I_{r+1} = I_0 \frac{[(1-\eta)(G_M+1)]^r}{1+\frac{I_0}{I_e}\left\{[(1-\eta)(G_M+1)]^r-1\right\}} \tag{48}$$

I_0 is the initial radiation intensity, due for instance to the spontaneous emission. An example of evolution of the laser signal in the cavity is presented in Fig. 22.

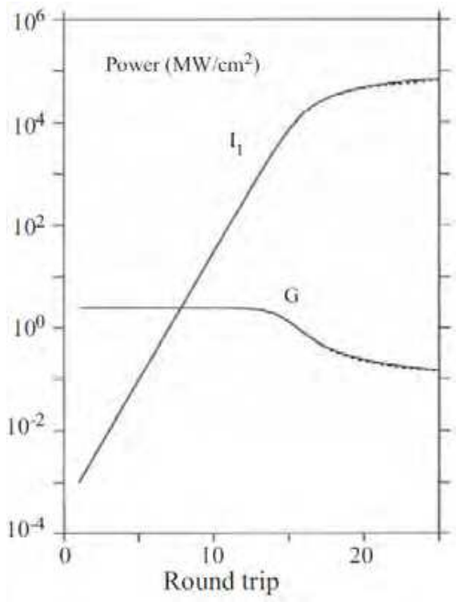

Fig. 22. Example of FEL signal evolution in the cavity up to saturation. Comparison between simulation (continuous line) and analytic calculation (dotted line). The lower curve represents the gain reduction due to the increase of the intracavity intensity.

The evolution is typically sigmoidal, as in the case of the conventional lasers.

We discuss the mechanism of mode-locking in the case of oscillator FEL. From the gain curve, whose width is given by:

$$(\Delta f)_{FEL} = \frac{c}{2N\lambda} \tag{49}$$

can be retrieved the number of coupled modes:

$$N_m = \frac{(\Delta f)_{FEL}}{(\Delta f)_e} = \frac{L}{N\lambda} \tag{50}$$

It is worth noticing that such value is inversely proportional to the slippage $N\lambda$. The physical meaning of this relation will be discussed later. In the absence of a specific mechanism of coupling of the longitudinal modes, the oscillator FEL modes also oscillate independently producing a fluctuating output radiation. But in the case of oscillator FEL, there is a natural coupling mechanism, resulting from the electron packets themselves, delivered by the accelerator with a pulse train structure of finite duration.

In Figure 23 is illustrated the structure of an electron beam delivered by a Radio-Frequency accelerator, which consists of a series of macro pulses themselves composed by a train of micro pulses which we assume to be Gaussian ($f(z) = \frac{1}{\sqrt{2\pi}\sigma_z} e^{-\frac{z^2}{2\sigma_z^2}}$.)

The current of a micro pulse corresponds to the peak current, while the current of the macro pulse corresponds to the average current. The case is similar to the one discussed for pulses in conventional lasers.

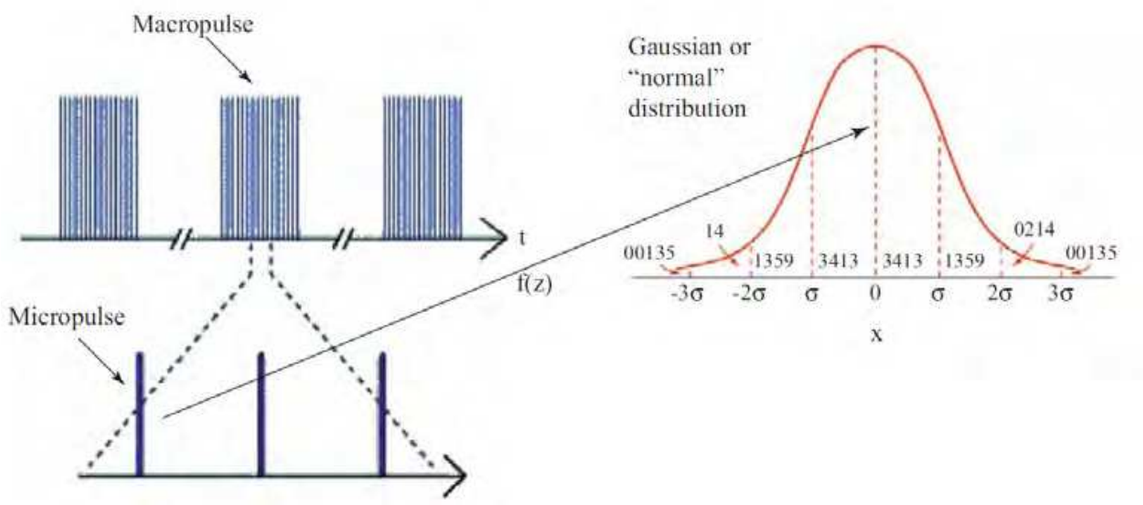

Fig. 23. Structure of an electron beam delivered by a Radio-Frequency accelerator

The gain process is determined by micro pulses and is therefore highly dependent on the electron beam finite distribution. As illustrated in Fig. 24, if the FEL process is determined by a pulsed electron beam structure, each packet of electrons will provide a packet of radiation. This is the basis of the FEL mode-locking mechanism. In order to understand it, the electron beam pulse must be considered as a gain filter.

This can be done considering the Fourier transform of the electron beam in the frequency domain of the FEL

$$\tilde{f}(\nu, \mu_c) = \frac{1}{\sqrt{2\pi}} \int_{-\infty}^{\infty} f(z) e^{-i(k-k_0)z} dz \tag{51}$$

$$= \frac{1}{\sqrt{2\pi}} \int_{-\infty}^{\infty} f(z) e^{-i\frac{\nu}{N\lambda}z} dz \, , \propto \frac{1}{\sqrt{2\pi}\mu_c} e^{-\frac{\nu^2}{2\mu_c^2}}, \quad \mu_c = \frac{\Delta}{\sigma_z}; \Delta = N\lambda$$

Δ is referred as the slippage length. The Fourier transform of *f(z)* is Gaussian too and in the following, we will use the normalized form: $\tilde{f}(\nu,\mu_c)=\frac{1}{\sqrt{2\pi}\mu_c}e^{-\frac{\nu^2}{2\mu_c^2}}$

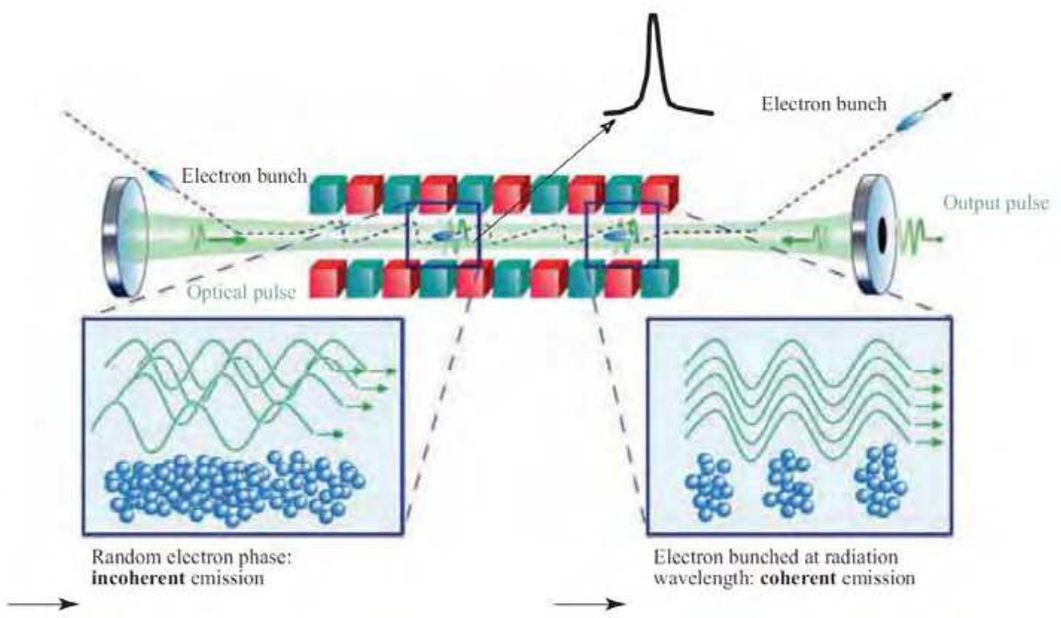

Fig. 24. Formation of a laser pulse from an electron beam pulse

The filter, representing the electron beam, is therefore regulated by the quantity μ_c, referred as longitudinal coupling coefficient. This quantity has an all-purpose physical meaning, which will be discussed in detail later. Here, we just highlight that when μ_c increases, the number of coupled modes increases, and that for a continuous beam ($\sigma_z \to \infty$) the operation becomes essentially single mode. The distribution derived from the former equation becomes a Dirac peak. The gain "filtered" by the electron beam can be written in terms of a convolution:

$$G_p(\nu,\mu_c)=\int_{-\infty}^{\infty}G(\nu+y)\tilde{f}(y,\mu_c)dy=2\pi g_0\int_0^1 t(1-t)sin(\nu t)e^{-(\mu_c t)^2/2}dt \quad (52)$$

It appears from this relation that for positive coupling coefficient values, the gain is decreased, simply because there are more modes oscillating in phase, and according to Eq. (52) that those coupled modes are within the rms band: $\sigma_\nu \cong \mu_c$.

5. FEL equations

The previous considerations are essentially qualitative, to make the forthcoming arguments quantitative we cast the FEL field evolution equation in the form

$$\frac{da}{d\tau}=i\pi g_0\int_0^\tau \tau' a(\tau-\tau')e^{-i\nu\tau'}d\tau' \quad a_n=|a_n|e^{i\phi_n}\ ,|a|^2=8\pi^2\frac{I}{I_s} \quad (53)$$

The previous equation can be exploited to specify the field growth before the saturation. It must be stressed that it contains something more, with respect to the considerations leading to the definition of the gain curve derived in the previous section, which were based on the assumption that the field remains constant during the interaction inside the undulator. Eq. (53) holds under more general assumptions, it includes the effects of high gain, i.e. the corrections associated to the fact that the field can vary significantly during the interaction. The FEL gain is the relative variation of the input field in one interaction ($G = \frac{|a|^2 - |a_0|^2}{|a_0|^2}$).

The FEL gain curve can be derived from Eq. (88), using the low gain approximation satisfactory for small signal gain coefficient values lower than 30%. For higher values, the gain curve is no more anti-symmetric. The maximum gain is no more simply proportional to g_0 and further corrections should be included, namely

$$G_M = G(g_0) \cong 0.85 g_0 + 0.192 g_0^2 + 4.23 \times 10^{-3} g_0^3, g_0 \le 10 \tag{54}$$

Eq. (53) considers an ideal electron beam, i.e. one with all electrons at the same energy. In reality, the energy distribution of the electron beam can be assumed Gaussian: $f(\varepsilon) = \frac{1}{\sqrt{2\pi}\sigma_\varepsilon} e^{-\frac{\varepsilon^2}{2\sigma_\varepsilon^2}}$, $\varepsilon = \frac{\gamma - \gamma_0}{\gamma_0}$, with σ_ε being the electron beam relative energy spread. The energy distribution induces an analogous distribution in the frequency domain of the FEL gain:

$$\tilde{f}(\nu, \mu_\varepsilon) = \frac{1}{\sqrt{2\pi}(\pi\mu_\varepsilon)} e^{-\frac{\nu^2}{2(\pi\mu_\varepsilon)^2}}, \quad \mu_\varepsilon = 4N\sigma_\varepsilon \tag{55}$$

Following the same procedure of convolution, as in the case of the longitudinal modes distribution, Eq. (53) is modified as following:

$$\frac{\partial a}{\partial \tau} = i\pi g_0 \int_0^\tau \tau' a(\tau - \tau') e^{-i\nu\tau'} e^{-\frac{1}{2}(\pi\mu_\varepsilon\tau')^2} d\tau' \tag{56}$$

The reduction of the gain due to the energy distribution is similar to the reduction of the gain due to the inhomogeneous broadening in conventional lasers and the parameter μ_ε is one of the inhomogeneous broadening parameter of the FEL. The reduction of the gain due to such effect can be quantified according to $G \cong \frac{G_M}{1 + 1.7\mu_\varepsilon^2}, \mu_\varepsilon << 1$. Further sources of inhomogeneous broadening will not be considered here.

The inclusion of the electron packet shape and of the consequent optical pulse phenomenology can be done by taking into account the fact that the photon packet, having a higher velocity that the electrons, slips over the electron packet (see Fig. 38). Therefore, Equation (56) should be modified according to:

$$\frac{\partial a(z,\tau)}{\partial \tau} = i\pi g_0 (z + \Delta\tau) \int_0^\tau \tau' a(z + \Delta\tau', \tau - \tau') e^{-i\nu\tau'} e^{-\frac{1}{2}(\pi\mu_\varepsilon\tau')^2} d\tau' \tag{57}$$

$g_0(z+\Delta\tau)$ is the small signal gain coefficient which takes into account the electrons distribution $f(z)$, $f(z)=\frac{1}{\sqrt{2\pi}\sigma_z}e^{-\frac{z^2}{2\sigma_z^2}}$. and the slippage. The former equation is sufficiently general to describe the dynamics of the pulse propagation with the effects of a high gain.

The coupling parameter μ_c has an additional physical meaning which is worth mentioning: it measures the overlapping of the electron beam with the photon beam. A very short electron beam remains superimposed to the photon beam for a very short time, which drives another reduction of the gain. The reduction of the gain due to the multi-mode coupling and spatial overlap can be quantified as following[4]: $G \cong \frac{G_M}{1+\frac{1}{3}\mu_c}$.

An important aspect of the FEL dynamics is the non-linear harmonic generation, resulting from the bunching mechanism, which itself is a consequence of the energy modulation mechanism (see Fig. 25). When the electrons are micro-bunched at a wavelength which corresponds to a submultiple of the fundamental wavelength, coherent emission is produced at higher order harmonics, throughout the mechanism of nonlinear harmonic generation.

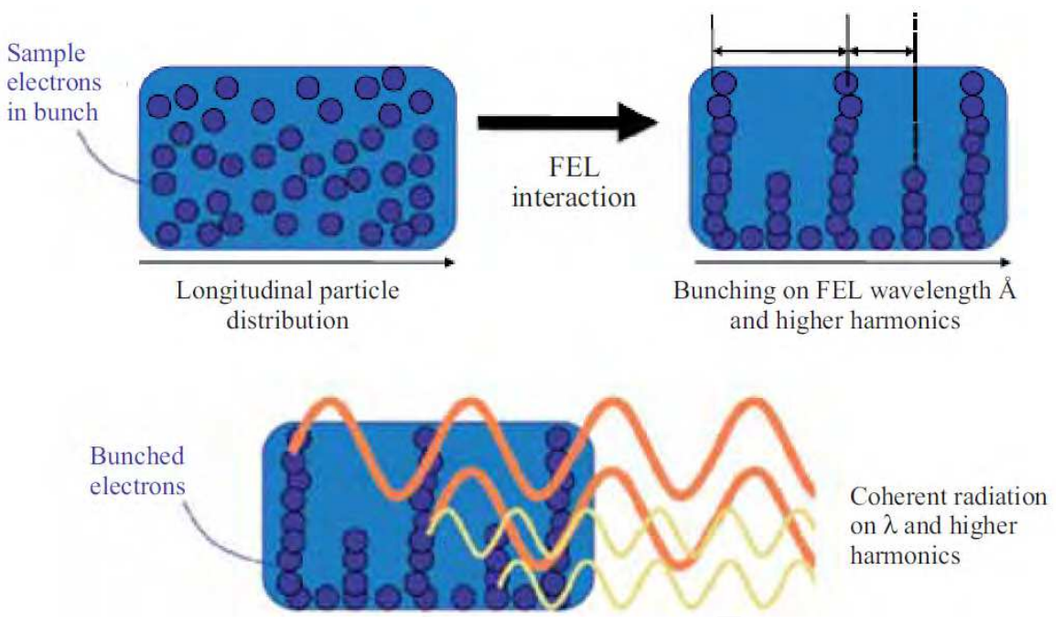

Fig. 25. Bunching mechanism induced by the FEL interaction. Bunching is performed at the resonant wavelength and on higher harmonics, allowing radiation production on the fundamental and higher harmonics

The intra cavity evolution of the fundamental and of the higher order harmonics is presented in Fig. 26.

[4]Both Eqs. (97) and (100) are valid in the case of small gain ($g_0 < 0.3$). For more general hypothesis, the expressions are slightly more complicated and will not be reported here for simplicity.

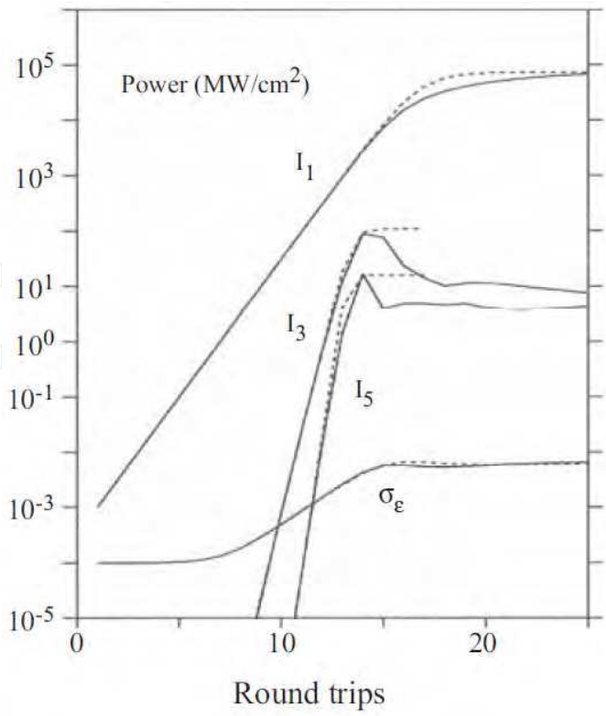

Fig. 26. Example of intra cavity evolution of the fundamental and of the high order harmonics (third and fifth). The Figure also reports the energy spread increase. Continuous lines: numerical calculation. Dashed line: analytical approximation

The dynamics of the process is understood as follows: the fundamental increases, until it reaches a sufficiently high power level to induce a bunching, that can lead to non-linear harmonic generation. The saturation mechanism comes from the combined effects of the energy loss and energy spread increase of the electron beam due to the same interaction. The maximum harmonic power is related to the maximum of the fundamental power according to[5]:

$$P_n^* = \frac{1}{2}\frac{\sqrt{n}}{n^3}\sqrt{\frac{n-1}{2}}g_{0,n}\frac{P_E}{4N} \tag{58}$$

where $g_{0,n}$ is the small signal gain coefficient of the harmonic n. Note that the coefficient $\frac{P_E}{4N}$ is the maximum power P_L achievable on the fundamental. The higher order harmonics, opposite to the fundamental, are not stored in the cavity. Therefore the powers presented in Fig. 26 are relative to the harmonic generation in one single round trip.

The non-linear harmonic generation mechanism is similar to the frequency-mixing mechanism in the case of non-linear optics. Eq. (58) can be understood as the non-linear response of the medium (the electron beam) to the laser electric field, so that it can then be written in terms of amplitude of the harmonics electric field:

[5]Note that in the linear polarized undulators, radiation is emitted on-axis only at odd order harmonics (3,5…)

$$E_n^* = \chi_n E_L \tag{59}$$

$$\chi_n = \sqrt{\frac{g_{0,n}}{2}\frac{\sqrt{n}}{n^3}\sqrt{\frac{n-1}{2}}}$$

Before concluding this paragraph, we will describe the profile of the pulses in a FEL oscillator and the method which can be implemented to shape the pulses simply using the cavity parameters.

7. Self amplified spontaneous FEL

One of the limiting factors of the FEL oscillator are the mirrors, which restrict the spectral range to wavelengths longer than a few hundreds of nm. Therefore, the soft X-ray region seems out of the range of operation of the FEL oscillator. It is possible to implement high gain mechanism which enables to reach saturation in one single pass in the undulator. One possible scheme is given in Fig. 27. A high peak current electron beam is injected in a long undulator, and amplifies the signal emitted in the first periods of the undulator. Such FEL configuration is referred as Self Amplified Spontaneous Emission (SASE) FEL. The main steps of the process are: Spontaneous emission, Energy modulation, Longitudinal bunching of the electrons over a distance of the order of the spontaneous radiation wavelength, Coherent emission, Saturation

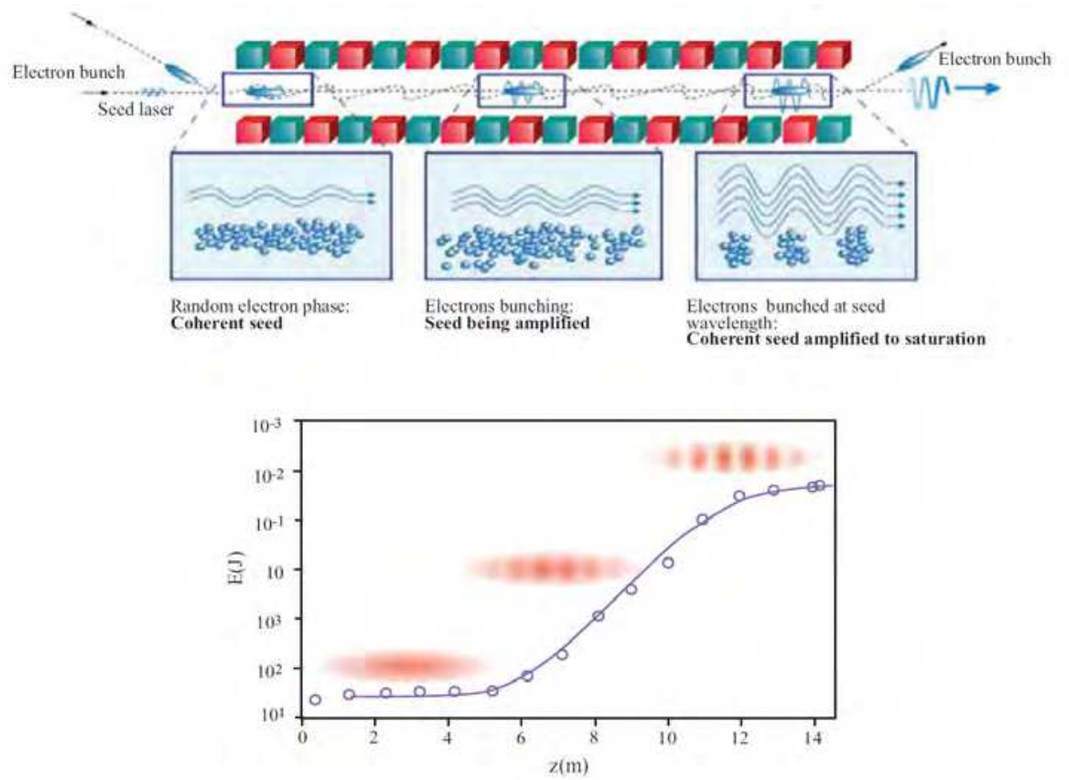

Fig. 27. SASE FEL process. Microscopic image of the bunching mechanism and laser signal increase along the undulator

In order to understand these steps, we go back to the integral form of the FEL equations (see Eq. (53)), which can be rewritten as follows:

$$e^{i\nu\tau}\frac{\partial a}{\partial \tau} = i\pi g_0 \int_0^{\tau} (\tau - \tau') a(\tau') e^{i\nu\tau'} d\tau' \tag{60}$$

$$e^{i\nu\tau}\frac{da}{d\tau} = i\pi g_0 \hat{D}_\tau^{-2}[a(\tau)e^{i\nu\tau}]$$

D_τ^{-2} indicates an integration (or a negative derivative) repeated twice.

We also used the following Cauchy equality for the integrations
($\hat{D}_x^{-n} f(x) = \frac{1}{(n-1)!}\int_0^x (x-\xi)^{n-1} f(\xi) d\xi$, $\hat{D}_x^{-n} f(x) = \int_0^x dx_1 ... \int_0^{x_n - 1} dx_n f(x_n)$).

Deriving both parts of Eq. (60) with respect to the temporal variables, the former integral equation can be transformed into an ordinary third order equation:

$$(\hat{D}_\tau^3 + 2i\nu\hat{D}_\tau^2 - \nu^2\hat{D}_\tau)a(\tau) = i\pi g_0 a(\tau)$$

$$\hat{D}_n^n = \frac{d^n}{d\tau^n} \tag{61}$$

$$a|_{\tau=0} = a_0, \hat{D}_\tau a|_{\tau=0} = 0, \hat{D}_\tau^2 a|_{\tau=0} = 0$$

The solution of this equation is obtained with a standard method and can be written as following:

$$a(\tau) = \frac{a_0}{3(\nu+p+q)} e^{-\frac{2}{3}i\nu\tau}((-\nu+p+q)e^{-\frac{i}{3}(p+q)\tau} +$$

$$+2(2\nu+p+q)e^{\frac{i}{6}(p+q)\tau}(cosh(\frac{\sqrt{3}}{6}(p-q)\tau)$$

$$+i\frac{\sqrt{3}\nu}{p-q}sinh(\frac{\sqrt{3}}{6}(p-q)\tau) \tag{62}$$

$$p = \left[\frac{1}{2}(r+\sqrt{d})\right]^{\frac{1}{3}}, q = \left[\frac{1}{2}(r-\sqrt{d})\right]^{\frac{1}{3}}$$

$$r = 27\pi g_0 - 2\nu^3, d = 27\pi g_0\left[27\pi g_0 - 4\nu^3\right]$$

It is not so easy to handle from the analytical point of view, nor easy to interpret from the physical point of view. A more transparent form can be obtained with ν =0 in Eq. (61). This is justified since we are considering solutions with a high gain, and that since in this case,

maximum gain is reached for small values of the detuning parameter. In the ν =0 case, Eq. (61) becomes much more simple:

$$\hat{D}_{\tau}^{3} a(\tau) = i\pi g_0 a(\tau) \tag{63}$$

The general solution is a linear combination of the three roots which is given by:

$$a(\tau) = \sum_{j=0}^{2} a_j R_j(\tau) = \sum_{j=0}^{2} a_j e^{\delta_j \tau} \tag{64}$$

δ_j are the three complex roots of $(\pi g_0)^{\frac{1}{3}}$. The solution is then finally given by:

$$a(\tau) \propto e^{(\pi g_0)^{\frac{1}{3}} \frac{\sqrt{3}}{2} \tau} \tag{65}$$

In addition, using $\tau = \frac{z}{N\lambda_u}$, the former relation becomes:

$$a(z) \propto e^{\frac{z}{2L_G}} \quad L_G = \frac{\lambda_u}{4\pi\sqrt{3}\rho} \quad \rho = \frac{1}{4\pi}\left(\frac{\pi g_0}{N^3}\right)^{\frac{1}{3}} \tag{66}$$

L_G is referred as the gain length, while ρ is referred as the Pierce parameter and constitutes one of the fundamental parameters of the SASE FEL. Finally, including the three roots in the expression, the evolution of the power in the small signal gain regime is given by:

$$|a(\tau)| = A(z)|a_0|^2, \; A(z) = \frac{1}{9}\left(3 + 2\cosh\left(\frac{z}{L_{g,1}}\right) + 4\cos\left(\frac{\sqrt{3}}{2}\frac{z}{L_{g,1}}\right)\cosh\left(\frac{z}{2L_{g,1}}\right)\right)$$

This relation enables to describe the initial zone of non-exponential growth.

The former equation only describes the intensity increase of the laser, not its saturation. The physical mechanism which determines the saturation is not different from the one which has been previously discussed in the case of the oscillators. To simplify the treatment, we assume that the evolution is just the one relative to the exponential growth, so that we can write the differential equation relative to the growth process as following:

$$\frac{d}{dz}P(z) = \frac{P(z)}{L_g}\left(1 - \frac{P(z)}{P_F}\right), \; P(0) = P_0$$

A quadratic non linearity has been added in order to take into account the effects of saturation. P_F indicates the final power in the saturation regime, that we will specify later. The solution of the former equation can be obtained easily, using the transformation: $\frac{d}{dz}T(z) = -\frac{1}{L_{g,1}}\left(T(z) - \frac{1}{P_{F,1}}\right), T(z) = \frac{1}{P_1(z)}$ and can be written:

$$P(z) = \frac{P_0}{9}\frac{e^{z/L_g}}{1 + \frac{P_0}{P_F}\left(e^{z/L_g} - 1\right)} \tag{67}$$

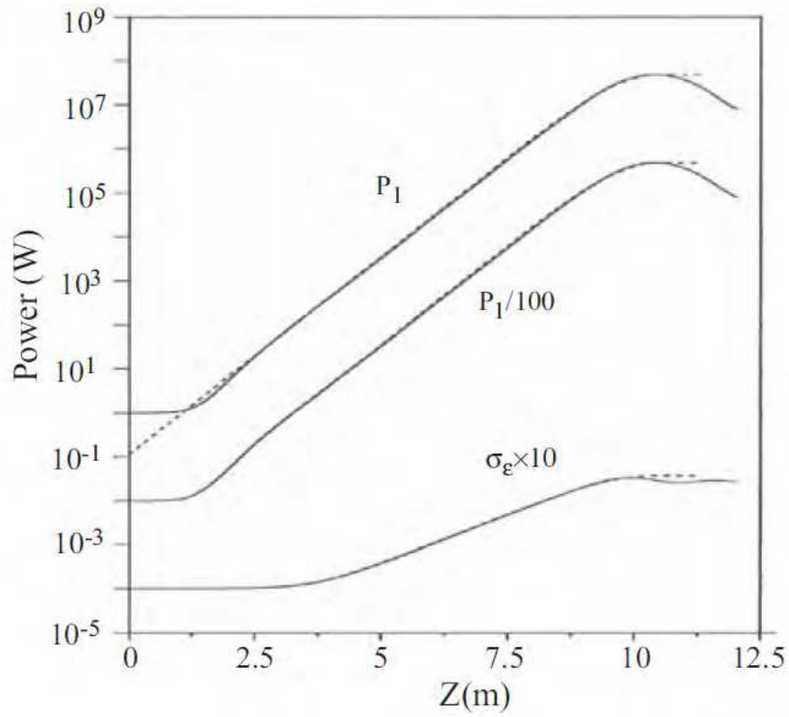

Fig. 28. Comparison between exact and approximated solutions, the upper curve represents the comparison with eq. (67) the mid curve provides the intensity growth (reduced by a factor 100 to avoid overlapping) predicted by eq. (68), the lower curve yields the evolution of the FEL induced energy spread.

In the more general case, the exponential is substituted by $A(z)$:

$$P(z) = \frac{P_0}{9} \frac{A(z)}{1 + \frac{P_0}{P_F}(A(z) - 1)} \tag{68}$$

The saturation power still remains to be defined. We already noted that when the gain coefficient increases, nonlinear elements tend to modify the maximum of the gain curve and its anti-symmetric shape.

$$G(\omega) = \frac{1}{\sqrt{2\pi}\rho} e^{-\frac{(\frac{\omega-\omega_0}{\omega_0})^2}{2\rho^2}}. \tag{69}$$

The relative width of the gain curve results proportional to the ρ parameter. According to what has been discussed in the former paragraphs, one expects the ratio between the FEL power and the electron beam power to be as well proportional to ρ.A more accurate analysis demonstrated that this is true, though with an additional numerical factor [6]:

$$P_F \cong \sqrt{2}\rho P_E \tag{70}$$

The saturation length is obtained by imposing $P(z) \cong P_F$ in Eq. (67), thus finding

$$Z_F = \ln\left(\frac{9P_F}{P_0}\right)L_g \tag{71}$$

Corresponding to the number of periods $N_F \cong \frac{1}{\rho}$

To get some numerical examples, we can note that if one limits the undulator length to a few tens of meters, given that the undulator period is of the order of a few centimetres and that $P_F \cong 10^8 P_0$, the value of the ρ results around 10^{-3}. A comparison between "analytical" and numerical predictions is given in Fig. 28.

8. SASE FEL and coherence

In the former paragraphs, we saw that the longitudinal coherence in FEL oscillators operated with short electron bunches, is guaranteed by the mode-locking mechanism. In the case of the FEL operated in the SASE regime, since there is no optical cavity, we can no longer talk about longitudinal modes, strictly speaking. Nevertheless, we can repeat the same argumentation on the filter properties of the electron beam to understand if something analogous to mode-locking can be defined for the cases of FEL operated in the SASE regime. As we already saw in the case of the oscillators, the effect of mode-locking is guaranteed in the interaction region where the electrons see a field with constant phase. This region is limited to one slippage length. We repeat the same procedure of Fourier transform which enabled to obtain Eq. (52). Using for the frequency domain the variable $\xi = \frac{\omega - \omega_0}{\omega_0}$ and changing the variable for the space domain according to $\tau = \frac{z}{c}$, Δ being the slippage length, we obtain the integral:

$$\tilde{f}(\xi) \propto \frac{1}{\sqrt{2\pi}}\int_{-\infty}^{\infty} f(\tau)e^{-i\xi\tau}d\tau \tag{72}$$

from which:

$$\tilde{f}(\xi) = \frac{1}{\sqrt{2\pi}\,\tilde{\mu}_c}e^{-\frac{\xi^2}{2\tilde{\mu}_c^2}} \quad \tilde{\mu}_c = \frac{\lambda}{\rho\sigma_z}$$

We used the approximation $\rho \cong \frac{1}{N}$. The former relation ensures that a coherence length l_c exists and that it is around λ/ρ (a more correct definition will be given later). If the electron beam length is about the coherence length, there would not be any problem of longitudinal coherence because all the modes inside the gain curve would be naturally coupled. Since in practical cases $\lambda/\rho << \sigma_z$ and since there is no clear definition of the longitudinal modes, we should define "macro modes", i.e. a sort of extension of the longitudinal modes. The number of "macro modes" is given by:

$$M_L \cong \frac{\sigma_z}{l_c} \tag{73}$$

Such macro modes introduced in the FEL Physics at the end of the 70's by Dattoli and Renieri are referred as *supermodes* (see [4] and references therein).

Each of these modes have a spatial distribution given by:

$$m(z) \cong \frac{1}{\sqrt{2\pi} l_c} e^{-\frac{z^2}{2l_c^2}}, \quad l_c = \frac{\lambda}{4\pi\sqrt{3}\rho\sigma_z}$$

The relevant Fourier transform $\tilde{m}(\xi)$ provide us with the frequency distribution. The total spectrum is given by:

$$S(\xi) = \sum_{n=1}^{M_L} \tilde{m}_n(\xi) \tag{74}$$

The phase of each component is totally random. The spatial distribution of the optical pulse is given by the Fourier transform of the spectrum and the results is shown in Fig. 29.

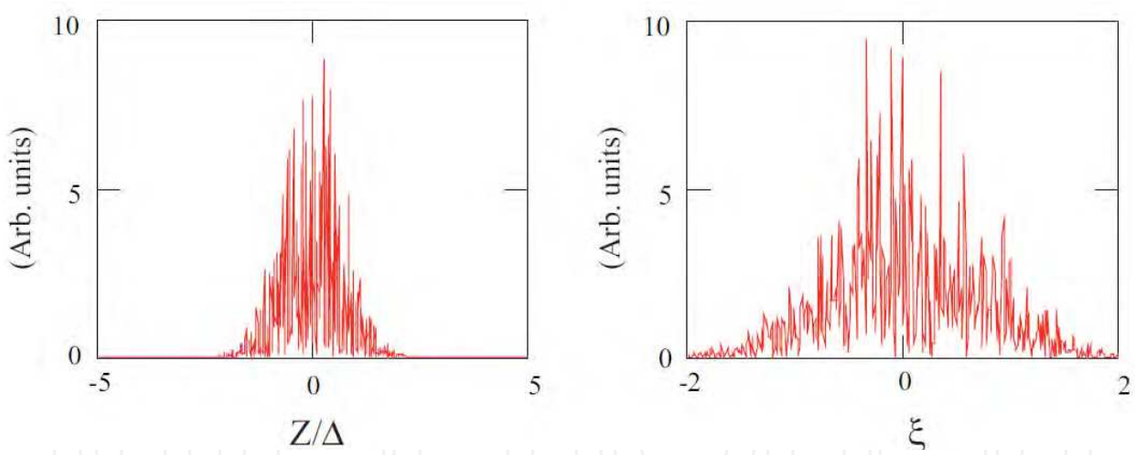

Fig. 29. Temporal and spectral distribution of the SASE FEL

Each randomly phased supermode makes one optical pulse which results in a series of spikes separated by a fixed distance: the coherence length (see Fig. 30).

The evolution of each supermode is nearly independent from the others. There is only the slippage which enables to create a coherence zone (of the same order of the coherence length) and produces a sort of smoothing of the chaos, while the field increases along the undulator (see Fig. 31).

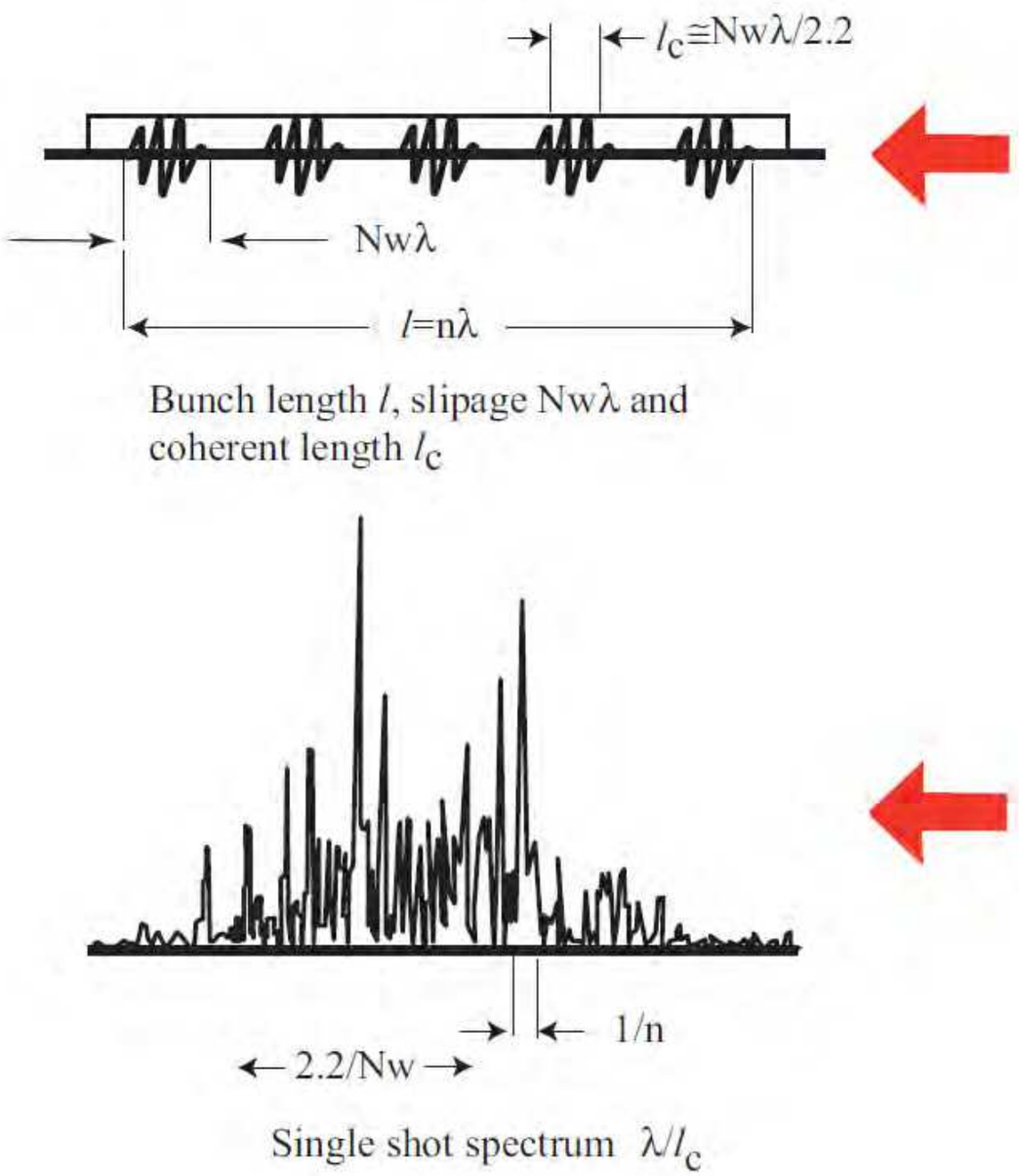

Fig. 30. Coherence length and spikes distribution

Dealing with a partially chaotic phenomenon, we should also define a probability distribution of the energy of these spikes [7]:

$$P(E) = \frac{M^M}{(M-1)!} x^{M-1} e^{-Mx} \ , \ x = \frac{E}{\langle E \rangle}$$

Such distributions are shown in Fig. 32. it is obvious that, when the number of supermodes increases, the distribution narrows and the average quadratic deviation is $\sigma_E \cong \frac{1}{\sqrt{M}}$

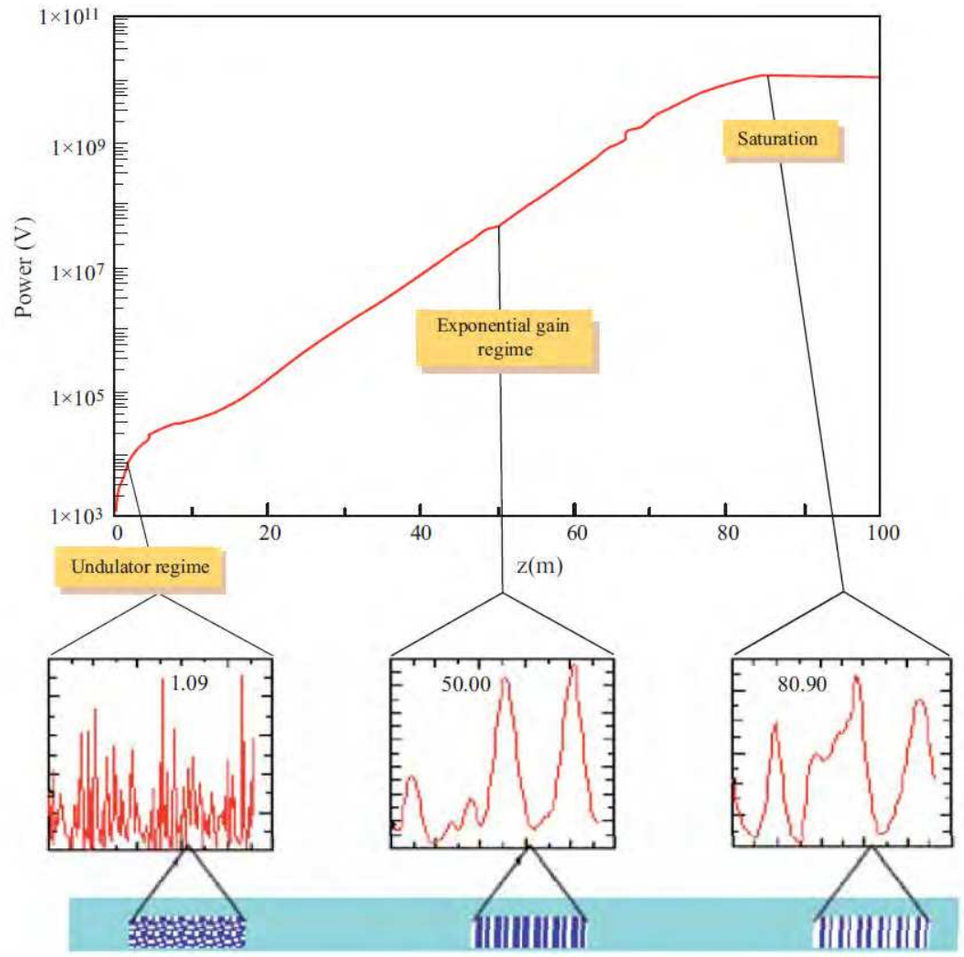

Fig. 31. Evolution of the power while signal increase and fluctuation smoothing

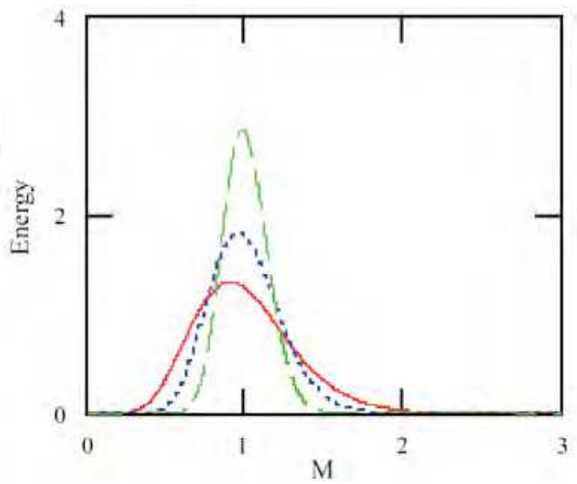

Fig. 32. Energy distribution of the FEL spikes as a function of $x = \frac{E}{\langle E \rangle}$, for various values of M. Continuous line: M=10, dotted line: M=20 and segmented line: M=50

Clarified the notion of longitudinal coherence, we move on to the definition of the transverse coherence. As previously, the problem of the definition of a transverse coherence results from the fact that there is no more optical cavity, which prevent us from defining strictly speaking transverse modes. We should note that in the high gain case, we will no longer be able to talk about free modes but guided modes, because of the strong distortion in the propagation caused by the interaction itself. An example of such behaviour is given in Fig. 33.

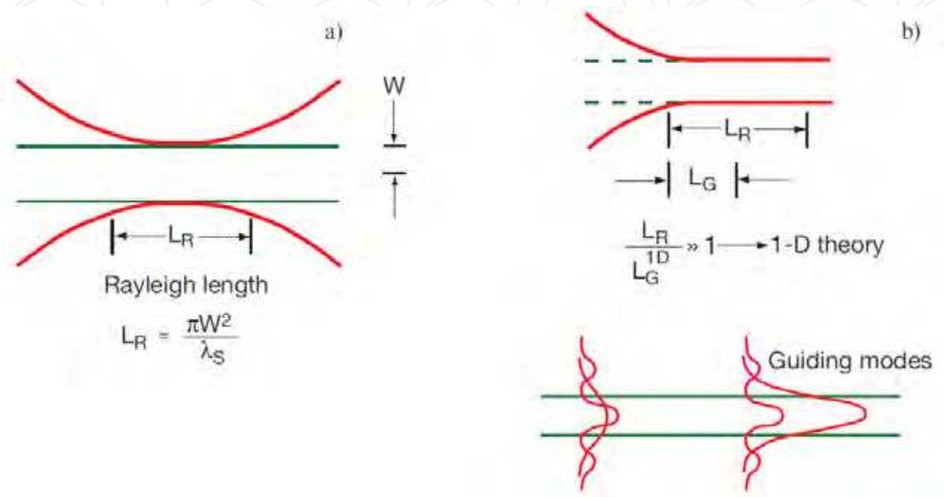

Fig. 33. a) Gaussian mode and b) guided mode

The Figure also illustrates the gain guiding mechanism, which becomes relevant as soon as the Rayleigh length becomes longer than the gain length. It is obvious that even in this case the ρ parameter plays a fundamental role. Indeed, the condition for the guided modes can be written as follows:

$$\rho >> \frac{\lambda_u \lambda}{4\pi^2 \sqrt{3} w_0^2} \tag{75}$$

Without optical cavity, the waist is essentially related to the transverse section of the electronic beam.

Before concluding this section, we note that the effects of inhomogeneous broadening and relative reduction of the gain in SASE can be treated using the same procedure given in the case of a FEL oscillator. In the case of energy spread, the parameter which quantifies the importance of the associated inhomogeneous broadening is

$$\tilde{\mu}_\varepsilon = \frac{2\sigma_\varepsilon}{\rho} \tag{76}$$

The macroscopic consequence is an increase of the saturation length given by:

$$\tilde{L}_g = \chi L_g \quad \chi = 1 + 0.185 \frac{\sqrt{3}}{2} \tilde{\mu}_\varepsilon^2 \tag{77}$$

The analysis of a SASE FEL system can then be done calculating quantities such as the saturation length and saturation power. One possible combination of the various parameters is given in Fig. 34, where we reported the saturation length, the power and the wavelength of a SASE FEL.

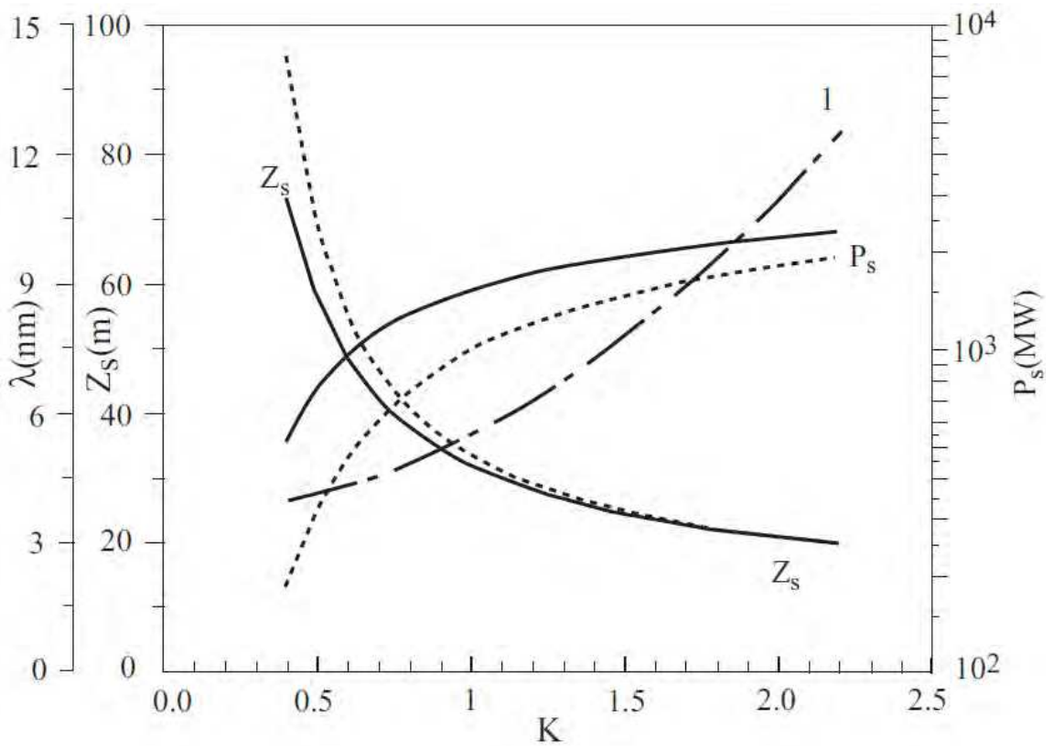

Fig. 34. Saturation length, power and wavelength as a function of the K parameter for a SASE FEL operating with a 2.8 cm period undulator and a 1 GeV energy, 5×10^{-4} energy spread and 1 kA current electron beam

9. FEL in the SASE regime and example of application

Several SASE FEL have been proposed as fourth generation light sources. These FEL will deliver radiation in the extreme ultraviolet and X-ray ranges, with a brightness at least 10 orders of magnitudes times larger than the one presently available on the synchrotron light sources. The evolution of the brightness in time is represented in Fig. 35. The so-called brightness is defined by *Number of photons per second per source unit area, per unit solid angle, per 0.1% bandwidth (photons / sec / mm^2 / mrad^2 / 0.1%$\Delta\omega$).*

The 10 orders of magnitude jump offered by the SASE FEL results from:

1. While conventional synchrotron light sources use the simple principle of spontaneous emission, SASE FEL are based on stimulated emission which guarantees a photon gain of $G=\frac{1}{9}e^{\frac{L_u}{\lambda_u}4\pi\sqrt{3}\rho}$, with $L_u=N\lambda_u$ the undulator length. Assuming $N\rho\cong 1$, one gets that with respect to the conventional sources, the photon flux is higher by roughly eight orders of magnitude.

2. The conventional sources use electron beams accelerated in a storage ring, while SASE FEL use an electron beam accelerated in a LINAC (linear accelerator) of high energy. The transverse dimensions of the emitting source (the electron beam) is therefore 100 times smaller in the case of the SASE FEL that in the case of the synchrotron sources. According to what has been said in (1) and given that the brightness is inversely proportional to the transverse section of the beam, the magnification factor reaches ten orders of magnitude.

Another interesting aspect of the SASE FEL is the pulse duration of the radiation: as illustrated in Fig. 36, SASE FEL can produce ultra-short radiation pulses.

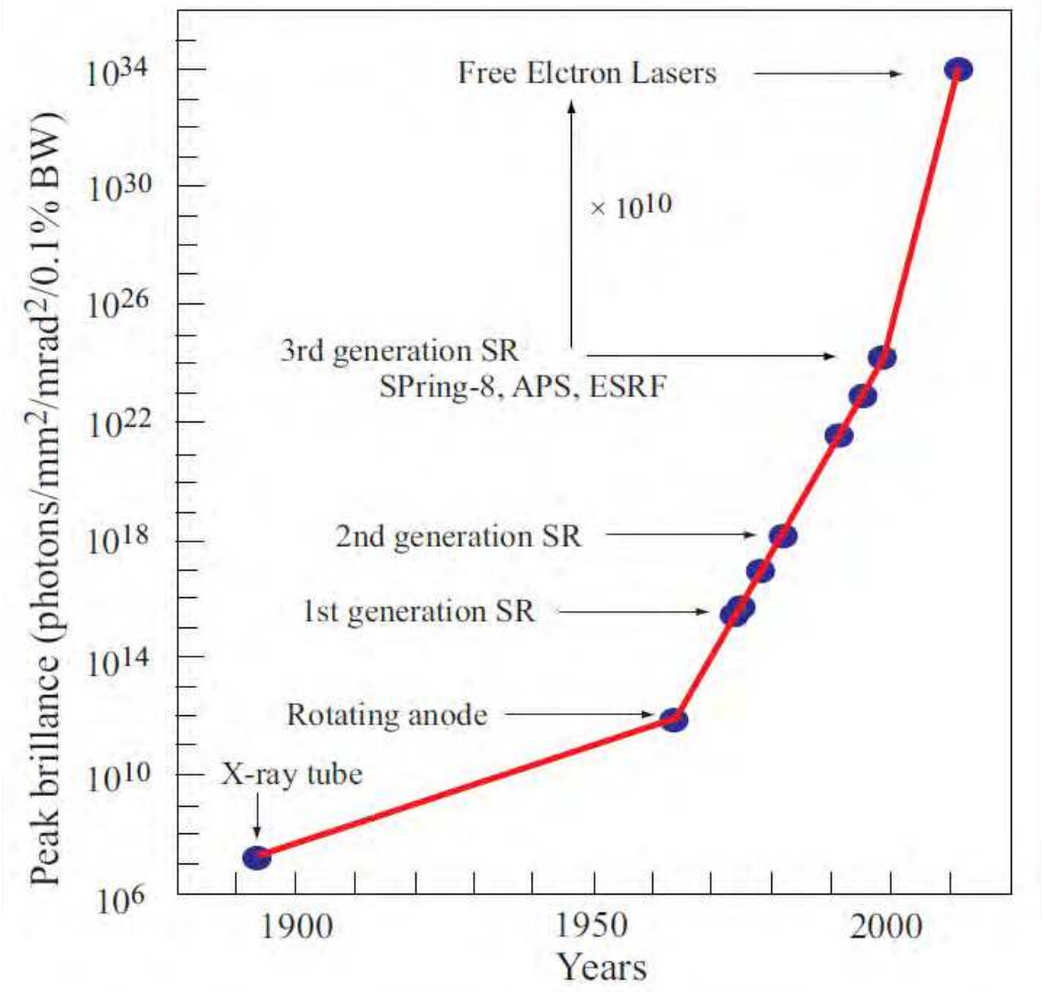

Fig. 35. Evolution of the brilliance of the X-ray conventional sources over the years and perspectives offered by FEL sources

The shortness of the X-ray pulse is related to the duration of the current pulse, which generated it. The electron beam length can be understood as follows. Assuming a maximum charge of 1 nC (10^{-9} C) and given that a SASE FEL needs currents of at least 1 kA to obtain a reasonable saturation length, it turns obvious that the duration of the electron beam should be smaller than a few ps.

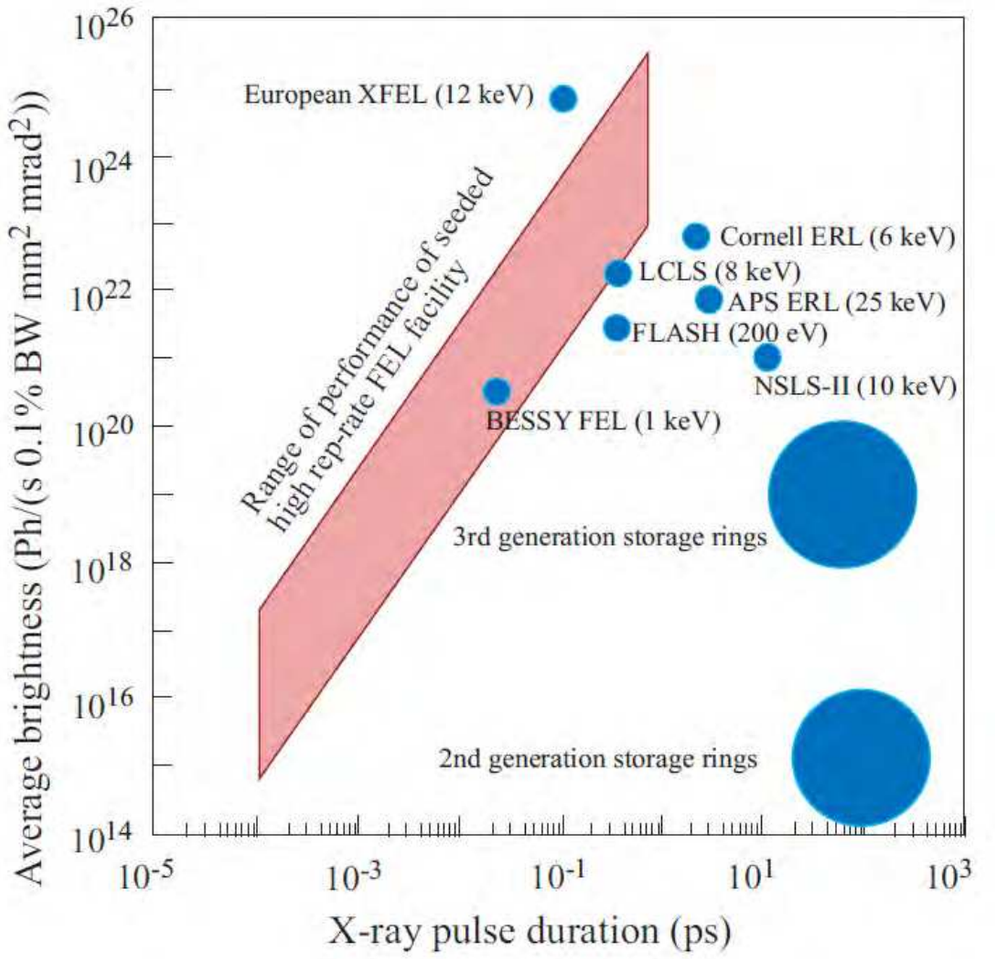

Fig. 36. Average brightness vs pulse duration of the SASE FEL sources

In conclusion: the SASE FEL can provide radiation in the X-ray range with duration of the order of the ps with extremely high brightness. Such characteristics make the SASE FEL sources of high interest for various types of applications.

10. References

[1] A. Yariv "Quantum Electronics", John Wiley and sons USA (1998)
[2] U. Kelly, *Ultrafast Laser Physics, Institute of Quantum Electronics, Swiss Federal Institute of Technology*. ETH (German: Eidgenössische Technische Hochschule) Höngerberg-HPT, CH-8093 Zürich, Switzerland.
[3] C.A. Brau, *Free-Electron Lasers*, Academic Press, Oxford (1990)
[4] G. Dattoli, A. Renieri, and A. Torre, *Lectures on Free Electron Laser Theory and Related Topics* (World Scientific, Singapore, 1993)
[5] F. Ciocci, G. Dattoli A. Torre and A. Renieri, *Insertion Devices for Synchrotron Radiation and Free Electron Laser* (World Scientific, Singapore 2000)
[6] G. Dattoli, P.L. Ottaviani, S. Pagnutti, *Booklet for FEL design: A collection of practical formulae*, ENEA Report RT/2007/40/FIM (2007)

[7] E.L. Saldin, E.A. Schneidmiller, M.V. Yurkov, *The Physics of Free Electron Lasers*, (Springer-Verlag Berlin 1999)

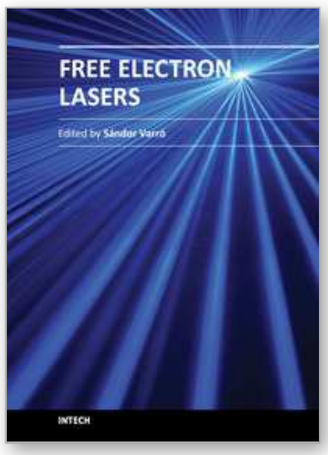

Free Electron Lasers

Edited by Dr. Sandor Varro

ISBN 978-953-51-0279-3
Hard cover, 250 pages
Publisher InTech
Published online 14, March, 2012
Published in print edition March, 2012

Free Electron Lasers consists of 10 chapters, which refer to fundamentals and design of various free electron laser systems, from the infrared to the xuv wavelength regimes. In addition to making a comparison with conventional lasers, a couple of special topics concerning near-field and cavity electrodynamics, compact and table-top arrangements and strong radiation induced exotic states of matter are analyzed as well. The control and diagnostics of such devices and radiation safety issues are also discussed. Free Electron Lasers provides a selection of research results on these special sources of radiation, concerning basic principles, applications and some interesting new ideas of current interest.

How to reference

In order to correctly reference this scholarly work, feel free to copy and paste the following:

G. Dattoli, M. Del Franco, M. Labat, P. L. Ottaviani and S. Pagnutti (2012). Introduction to the Physics of Free Electron Laser and Comparison with Conventional Laser Sources, Free Electron Lasers, Dr. Sandor Varro (Ed.), ISBN: 978-953-51-0279-3, InTech, Available from: http://www.intechopen.com/books/free-electron-lasers/free-electron-laser-devices-a-comparison-with-ordinary-laser-sources

INTECH
open science | open minds

InTech Europe
University Campus STeP Ri
Slavka Krautzeka 83/A
51000 Rijeka, Croatia
Phone: +385 (51) 770 447
Fax: +385 (51) 686 166
www.intechopen.com

InTech China
Unit 405, Office Block, Hotel Equatorial Shanghai
No.65, Yan An Road (West), Shanghai, 200040, China
中国上海市延安西路65号上海国际贵都大饭店办公楼405单元
Phone: +86-21-62489820
Fax: +86-21-62489821

IntechOpen